Mechanism and Machine Theory 122 (2018) 404–431

Contents lists available at ScienceDirect

Mechanism and Machine Theory

journal homepage: www.elsevier.com/locate/mechmachtheory

Research paper

Workspace characterization and kinematic analysis of general spherical parallel manipulators revisited via graphical based approaches

Khaled Assad Arrouk*, B. Chedli Bouzgarrou, Grigore Gogu

Pascal Institute, UMR6602 UBP/CNRS/SIGMA-Clermont BP10448, F63000 Clermont-Ferrand, France

ARTICLE INFO

Article history:
Received 31 July 2017
Revised 16 November 2017
Accepted 24 November 2017

Keywords:
Spherical parallel robotic manipulators (SPRMs)
3D total orientation workspace
Full-spin orientation workspace
Assembly modes
Forward kinematic problem (FKP)

ABSTRACT

This paper revisits some fundamental issues in kinematic analysis of spherical parallel robotic manipulators (SPRMs), such as the orientation capacities of the mobile platform (MPF), and assembly modes determination. The orientation capacities are analyzed by using several types of workspaces: total orientation workspace, full-spin orientation workspace, and constant-spin orientation workspace. The adopted representation of the MPF orientation brings up-to-date the use of the spherical coordinate system, which we find more appropriate when Euler angle orientation parameters are used. This representation is applied to each limb, considered independent from the rest of the mechanism and having the mobile platform as end-effector. The 3D orientation space reached by each limb, which is called also vertex space, is represented as a 3D solid volume. Thereafter, the operational space of the SPRM is directly determined by the Boolean intersection of the previously obtained volumes. Moreover, by fixing the joint space variables, the domain reached by each limb in the operational space is a surface. The Boolean intersection of the obtained surfaces is nothing but the set of points corresponding to the solutions of the forward kinematic problem. These operations are implemented in CAD software and the proposed approaches have been validated successfully by using several examples of application for both workspace determination and representation and FKP resolution.

1. Introduction

Workspace characterization is a fundamental issue in the design process of a robotic manipulator. For parallel manipulators, this remains a challenging problem due to the complexity of the direct kinematics. On the other hand, the orientation workspace is not well defined in the general case due to the non uniqueness of the orientation parameters for a given configuration. The orientation of a solid in the Euclidian space is given univocally by a rotation matrix which is an element of the Special Orthogonal group denoted by SO(3) [1]. As far as we know, there is no simple metric defined in SO(3) which allows measuring the volume of a 3D domain in the orientation space. This paper addresses the analysis of the orientation space with applications to the 3-RRR SPRM.

It is noteworthy before going further to point out that the state-of-the-art presented in this section will focus only on the SPRM 3-RRR-type, where R stands for a revolute joint, for both workspace determination and FKP resolution. For this

* Corresponding author.
E-mail address: khaled.arrouk@sigma-clermont.fr (K.A. Arrouk).

https://doi.org/10.1016/j.mechmachtheory.2017.11.019
0094-114X/

List of abbreviations and symbols

Abbreviation	*Meaning*
SCS	**s**pherical **c**oordinate **s**ystem
SPRMs	**s**pherical **p**arallel **r**obotic **m**anipulators
SSL	**s**erial **s**pherical **l**imb
PPRMs	**p**lanar **p**arallel **r**obotic **m**anipulators
FKM	**f**orward **k**inematic **m**odel
FKP	**f**orward **k**inematic **p**roblem
IKP	**i**nverse **k**inematic **p**roblem
CSOW	**c**onstant-**s**pin **o**rientation **w**orkspace
FSOW	**f**ull-**s**pin **o**rientation **w**orkspace
SO(3)	**s**pecial **o**rthogonal group
PRM-SM-MPF	**p**arallel **r**obotic **m**anipulators with **s**pherical **m**otion of the **m**oving **p**latform
PRMs	**p**arallel **r**obotic **m**anipulators
CAD	**c**omputer-**a**ided design
FB	**f**ixed **b**ase
MPF	**m**oving **p**latform
EE	**e**nd-**e**ffector
EECP	**e**nd-**e**ffector **c**haracteristic **p**oint
3D TOW	**3D t**otal **o**rientation **w**orkspace
DOW	**d**exterous **o**rientation **w**orkspace

Symbols	*Meaning*
O-$X_0Y_0Z_0$	operational absolute coordinate system fixed to the base.
E-$X_EY_EZ_E$	coordinate system fixed to the moving platform
ξ	angle between the plane X_0OY_0 and the axis of the first revolute joint of the spherical limb.
α	semi-angle of the conical surface. This surface is formed by the rotation axis of the passive revolute joints fixed on the MPF.
β_{1k} $k=(a, b, c)$	length of the proximal link situated between the actuated revolute joint attached to the FB and the subsequent passive intermediate revolute joint in the limb.
θ_{1k} $k=(a, b, c)$	joint parameters of a SSL.
ρ	radial distance calculated from O replacing the spin rotation angle.
M_k-$X_{1k}Y_{1k}Z_{1k}$ $k=(a, b, c)$	coordinate system attached to the first revolute joint in k limb mounted on the fixed base.
υ_k $k=(a, b, c)$	rotation angle around Z_0-axis of O-$X_0Y_0Z_0$ to reach the X_{1k}-axis of the first revolute joint in the limb.
γ	rotation angle around X_E of the coordinate system attached to the MPF for reaching the coordinate system attached to the vertices of the MPF.
β_{2k} $k=(a, b, c)$	length of the distal link situated between the passive intermediate revolute joint and the passive revolute joint attached to the MPF.
ϕ_Z, ϕ_y, ϕ_x	operational parameters of the robot defined by the three Euler angles.
h	the thickness equal to $(\rho_{max} - \rho_{min})$.

type of robot, the MPF of SPRMs can rotate around any axis passing through a fixed point, which is referred to as the center of the spherical motion of the MPF; the axes of all revolute joints of the SPRM intersect in this fixed point.

Several methods have been used for workspace analysis of SPRMs. In [2], authors have proposed a new analytical method to determine the workspace boundaries of symmetrical SPRMs. The method is based on the use of the tilt-and-torsion angles to visualize the orientation workspace as a subset of a solid cylinder. The method presented in [2] does not provide a calculation of the orientation workspace volume. However, the visualization of such workspace can indicate the size of the orientation workspace. In [3], a technique based on the Euler-Rodrigues parameters of the rotation of a rigid body is developed to determine the workspace of SPRM 3-$\underline{R}$RR-type. The authors have used a solid modeler to approximate the volume reached by each spherical serial limb by dividing this volume into several slices. Design optimization for a large workspace and dimensional synthesis of SPRMs has been reported in [4]. The synthesis procedure in this work utilizes an algebraic algorithm, based on the work originally proposed in [5], in order to define the workspace of the SPRM in the image space of spherical displacements. Authors in [5] have presented an approach based on the use of the Euclidean norm of the difference of the quaternions associated with the two poses of a rigid body under spherical motion. So, they define the distance between two different orientations in the Euclidean three-dimensional space E^3 as the magnitude of the difference between the corresponding quaternions.

The use of SCS in orientation workspace representation was coined by Benea in his Ph.D. thesis [6]. Author has used the pseudo-spherical representation for the determination of the orientation workspace of 6-DOFs PRMs 6-RKS-type. In [6] a discretization method based on the use of IKP has been used for this purpose.

This paper can be considered as extension of our previous works on workspace analysis of PPRMs [7] to SPRMs where graphical based techniques are exploited. For SPRMs, we adopt herein and in [8] a representation of the orientation workspace in a SCS as introduced in [6]. We find such a representation the most appropriate when Euler angles are used as orientation parameters. Our approach for workspace determination is characterized as following:

a. The 3D vertex spaces attainable by the EECP which lies on the MPF of the robot are obtained by discretizing the joint space of each SSL of the 3-RRR-type, having the MPF as end-effector, and using its forward kinematic model.
b. CAD functionalities have been used to reconstruct the 3D volumes associated with the vertex spaces reached by the SSLs.
c. The 3D TOW of 3-RRR SPRM is obtained by performing Boolean intersection operations on the 3D vertex volumes relative to the limbs.
d. Other types of orientation workspaces such as full-spin and constant-spin orientation workspaces are extracted from the 3D total orientation workspace.
e. Various workspaces analyses in this paper are based on graphical resolutions by using the functionalities of CAD environments.
f. Thanks to this 3D representation of the workspace, one can manipulate all views, display and explore any useful information in a user-friendly, interactive way.

The resolution of the FKP of SPRMs involves finding the orientation of the platform corresponding to given actuator input variables associated with the motorized rotation angles for SPRM 3-RRR-type. Owing to the multi-loop architecture of SPRMs, the FKP, in general, does not allow for closed-form solutions. In addition, the nonlinear system of trigonometric equations implies a high computational complexity [9]. Several analytical polynomial approaches have traditionally been used for resolving the FKP of SPRMs. The FKP, for SPRM 3-RRR-type, can be reduced to an eighth degree univariate polynomial resolution, which can be performed numerically [10,11]. All FKP solutions, associated with the assembly modes, correspond to the roots of 8th degree univariate polynomial equation. This latter is referred to as the SPRM characteristic equation. Gosselin et al. [10] have shown that this polynomial degree is minimal since 8 real solutions corresponding to actual configurations have been found for a given set of actuated joint variables. In [12,13], the authors reported a compact polynomial method based on a algebraic-analytical approach named *Kinematic Mapping Approach* to find all the solutions of the FKP of SPRMs 3-RRR-type. The contribution of the above reference lies in the use of kinematic mapping for the FKP, thereby reducing substantially the computational effort as compared to computations required by other analytical methods. In [14] the authors have used an analytical approach to solve FKP of the Agile Eye SPRM 3-RRR-type. For this spherical wrist, authors have demonstrated numerically that the four solutions associated with the FKP have a simple geometric relationship with its working modes associated with the eight solutions to the IKP of the Agile Eye mechanism. In [15], the authors have presented a method to solve the system of spherical kinematic constraints directly from the Denavit–Hartenberg parameters of the involved kinematic chains that relies on the properties of polynomials in Bernstein form. The FKP of SPRMs with n limbs was converted to solving systems of $n-1$ second-order multinomials. In [9], the SPRM has been divided into two four-bar spherical linkages which leads to FKP equations with compact coefficients, so the FKP equations can be solved semi-graphically. In [9], the rough estimates of the obtained solutions are submitted as initial guesses to a nonlinear equation solver for accurate solutions. Kong and Gosselin in [16] have proposed a formula that produces a unique solution to the FKP for a specific set of actuated joint variables for quadratic SPRMs.

The analysis of the above state-of-the-art on FKP resolution of SPRMs 3-RRR-type underlines the fact that the majority of the approaches used is mainly numerical and based on analytical polynomial approaches. These approaches have largely focused on the transformation of the FKP into a high-degree univariate polynomial using an elimination procedure. The different roots of the obtained polynomial correspond to the required solutions and are referred to as assembly modes. It is worth noting that the order of the univariate polynomial does not always represent the number of actual real solutions of the FKP of PRMs.

Different from these approaches, our procedure for FKP resolution and assembly modes definition is characterized as following:

a. Considering given values for rotation angles of the actuated revolute joints, the regions attained by the EECP which lies on the MPF of the robot is a 2D surface embedded in 3D vertex space associated with each isolated SSL having the MPF as EE. The surfaces represent the geometrical loci attainable by the EECP attached to each serial spherical limb having the MPF as EE.
b. The methodologies previously presented in the literature for FKP solving of SPRMs are based globally on the use of complex mathematical formulas relative to a polynomial of degree 8. This latter is derived from the geometric and kinematic constraint equations of robotic architecture closed loops. However, this is not the case in our proposed approaches which give designers the opportunity to cope with and overcome the calculation challenges related to the algebraic approach which depends generally on the use of a complex analytical equation system. We resort to a CAD-based graphical programming for FKP resolution. It is sufficient to perform intersection operation on the reconstructed free-from surfaces for obtaining all real solutions of the FKP of SPRM associated with the assembly modes.

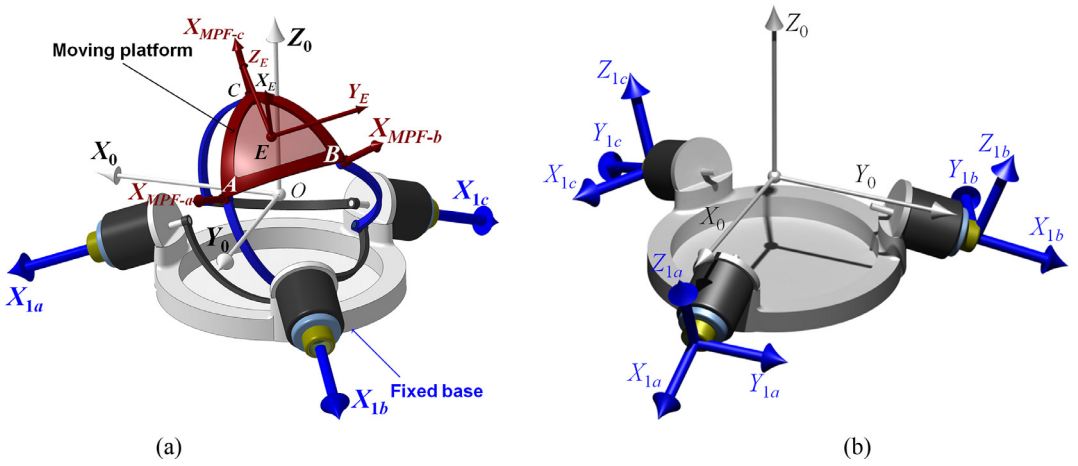

Fig. 1. CAD model of SPRM 3-RRR-type (a) and CAD model of the fixed base (b).

c. The geometrical approach for FKP resolution allows efficiently locating and simultaneously visualizing all FKP solutions within the different 3D types of workspace which we have defined in this work, such as 3D TOW and 3D FSOW.

Finally, it is noteworthy that, the propose methodologies for FKP resolution and workspace determination are on the track of our previous works based on geometrical approaches implemented in CAD tools [7,17,18]. In the same vein, our previous works treat the main kinematic and geometric problem for mainly **P**lanar **P**arallel **R**obotic **M**anipulator**s** (**PPRMs**). The methods presented in our earlier articles pertains to pure geometrical methodologies and emphasize the use of a CAD environment as a natural framework for considering the central problems related to geometric and kinematic analysis of PPRMs. The approaches proposed in our preceding works handles the geometric entities generated from a parametric design of PPRMs. This paper explores the potential of CAD tools for SPRMs.

This paper is organized as follows: in **Section 2**, a description and parameterizing of the architecture of the SPRM 3-RRR used in our study is given. **Section 3** presents the geometric modeling of the SPRM 3-RRR-type. **Section 4** introduces an appropriate representation of the orientation operational space of the SPRMs. In the same section, the FKP of a general design of SPRM is resolved. In **Section 5** we present the technique adopted with the aim of 3D TOW determination and representation of SPRM 3-RRR-type. **Section 6** presents some applications to workspace analysis of SPRM 3-RRR-type. It presents a set of techniques to obtain both CSOW and FSOW. In **Sections 4**, **5** and **6** several numerical examples are given to demonstrate the potential and applicability of the proposed methodologies for both FKP resolution and workspace determination and representation. Finally, some advantages of the proposed methodologies are presented in **Section 7**.

2. Parameterizing of the SPRM 3-RRR-type

A SPRM of 3-RRR-type (the underlined letter stands for the actuated revolute joint) is formed by a fixed base (FB) and a moving platform (MPF) which are connected through three limbs RRR-type. The SSLs RRR-type are, designated in our paper by the letters *a*, *b* and *c*, for the first, the second and the third leg respectively. Each SSL RRR-type has two links connected to each other by a revolute joint: a proximal link attached to the fixed base, and a distal link attached to the moving platform by revolute joints. The SPRM is characterized by the fact that all joint axes intersect at a common point, which is called the geometric center of the spherical mechanism or the center of rotation, which is referred to as *O*, as illustrated in Figs. 1 and 2. Figs. 1 and 2 display, respectively, a CAD model of a general SPRM 3-RRR-type having three rotational DOFs, and an SSL isolated from the rest of the mechanism. These figures include the notations used throughout the paper. In this section the parameterizing of the SPRM 3-RRR-type is given by introducing several sets of parameters, as it is explained below. For this purpose, we define, first of all, two coordinate systems: the first is the absolute coordinate system fixed to the base O-$X_0Y_0Z_0$ where point O represents the geometric center or the rotation center of the SPRM 3-RRR-type. The second coordinate system is E-$X_EY_EZ_E$, fixed to the moving platform (Figs. 1–3).

We define five sets, **Set-*i*** with $i=1$–5, of parameters involved in the geometric model formulations including: the parameters of the FB (**Set-1**), the parameters of the MPF (**Set-2**), joint and geometric design parameters of each limb k (with $k=a, b, c$) (**Set-3**), motorized joint parameters of the SPRM 3-RRR-type (**Set-4**), orientation operational space parameters of the SPRM 3-RRR-type (**Set-5**).

Set-1 is defined using the intrinsic parameters (ξ, υ_k), ($k=a, b, c$) that depend on the geometric design of the SPRM, see Fig. 2. These parameters allow transformation from the fixed base coordinate system O-$X_0Y_0Z_0$ to the one attached to the revolute joint M_k-$X_{1k}Y_{1k}Z_{1k}$ by considering each motor k mounted on the fixed base, as displayed in Fig. 1(b), where, υ_k ($k=a, b, c$) designate the first rotation angle around Z_0-axis of O-$X_0Y_0Z_0$. The values of this parameter, for the SPRM under study, are as follows in Fig. 2(b): $\upsilon_a=0$, $\upsilon_b=120$ (deg), $\upsilon_c=240$ (deg). The parameter ξ stands for the rotation angle

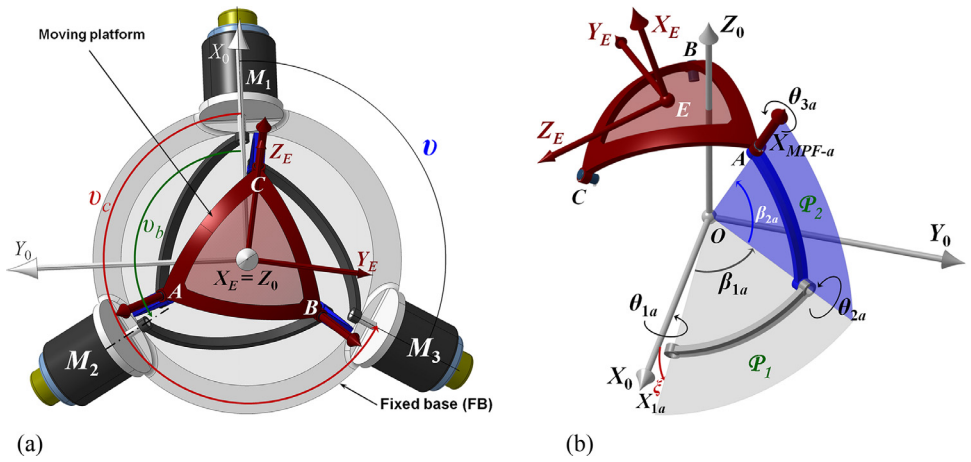

Fig. 2. Top view of SPRM 3-RRR-type (a), parameterized CAD model of one serial spherical limb RRR-type (b).

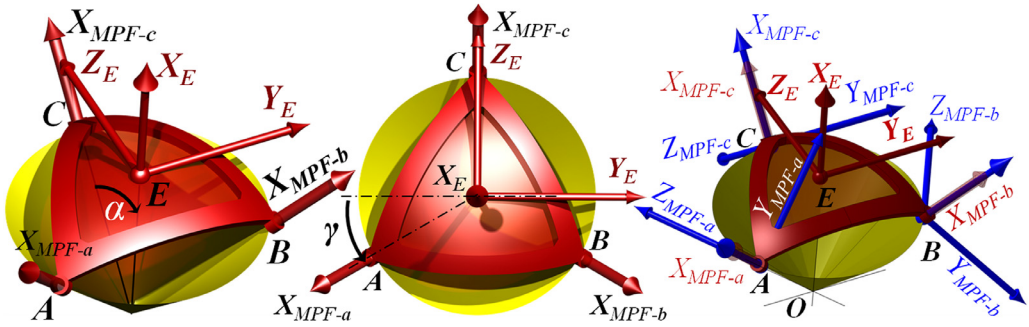

Fig. 3. CAD model of the MPF and 3D view of the travel from E–$X_EY_EZ_E$ to the coordinate systems attached to the vertices of the MPF.

around Y_{0k}. It is the angle between the plane X_0OY_0 and the axis of the first revolute joint of each SSL, see Fig. 2(b). These two rotations allow the motorized revolute joint axis X_{1k} of each limb with ($k = a, b, c$) to be attained.

Set-2 includes the intrinsic parameters of the MPF. This set is defined, similarly to **Set-1**, using two parameters (α, γ_k) that depend also on the geometric design of the SPRM, see Fig. 3. These parameters allow travel from the MPF coordinate system E-$X_EY_EZ_E$ to those attached to the three vertices (A, B, C) of the MPF, as depicted in Fig. 3.

In **Set-2**, α indicates the semi-angle of the conical surface formed by the rotation axis of the passive revolute joints fixed on the MPF. Also, γ_k ($k = a, b, c$) designate the rotation angles around X_E of the coordinate system attached to the MPF, as displayed in Fig. 3. Given that the base of the trihedral associated with the MPF is an equilateral triangle, see Fig. 3, we have $\gamma_a = \pi/6$, $\gamma_b = \pi/6$ and $\gamma_c = 0$.

Set-3 contains the joint and design parameters of a SSL RRR-type. The geometry of each SSL is defined by two angles: β_{1k} and β_{2k}. Where, β_{1k} ($k = a, b, c$) stands for the length of the proximal link situated between the actuated revolute joint attached to the fixed base and the subsequent passive intermediate revolute joint. Similarly, the length of the distal link, situated between the passive intermediate revolute joint and the subsequent passive revolute joint attached to the moving platform, is defined by the angle β_{2k} with ($k = a, b, c$), see Fig. 2(b). In addition, the configuration of a serial spherical leg k, (with $k = a, b, c$), in accordance with Fig. 2(b), is given by the set of parameters θ_{1k}, θ_{2k} and θ_{3k}.

Set-4 regroups the actuated revolute joints parameters. These parameters are denoted by θ_{1a}, θ_{1b} and θ_{1c}.

Set-5 is formed by the operational space orientation parameters of the SPRM 3-RRR-type. These parameters are the three Euler angles ϕ_Z, ϕ_y and ϕ_x relative to the sequence ZYX of successive rotations from the frame of reference O-$X_0Y_0Z_0$ to the frame attached to the mobile platform E-$X_EY_EZ_E$. Thus, the rotational matrix describing the orientation of the mobile platform can be written as follows Eq. (1):

$$\mathbf{R}_{oE} = \mathbf{R}_{Z0}(\phi_Z)\,\mathbf{R}_{Y1}(\phi_y)\,\mathbf{R}_{X2}(\phi_x) \tag{1}$$

$\mathbf{R}_{Z0}(\phi_Z)$ stands for the rotation matrix corresponding to a rotation about axis OZ_0 at angle ϕ_Z
$\mathbf{R}_{Y1}(\phi_y)$ stands for the rotation matrix corresponding to a rotation about axis OY_1 at angle ϕ_y
$\mathbf{R}_{X2}(\phi_x)$ stands for the rotation matrix corresponding to a rotation about axis OX_2 at angle ϕ_x

Table 1
Parameters of SPRM 3-RRR-type.

Parameter sets	Intrinsic parameters of FB	Intrinsic parameters of MPF	Geometric design of limb $k = a, b, c$	Joint parameters of the limb $k = a, b, c$			Angles of motorized revolute joints			Operational parameters of the robot		
Symbol	ξ	α	β_{1k}	θ_{1k}	θ_{2k}	θ_{3k}	θ_{1a}	θ_{1b}	θ_{1c}	ϕ_z	ϕ_y	ϕ_x
	$\upsilon_a, \upsilon_b, \upsilon_c$	$\gamma_a, \gamma_b, \gamma_c$	β_{2k}									

From Eq. (1) one can obtain the global rotation matrix of the mobile platform with respect to the fixed base:

$$\mathbf{R}_{oE} = \begin{bmatrix} c_{\phi z}\, c_{\phi y} & -s_{\phi z}\, c_{\phi x} + c_{\phi z}\, s_{\phi y}\, s_{\phi x} & s_{\phi z}\, s_{\phi x} + c_{\phi z}\, s_{\phi y}\, c_{\phi x} \\ s_{\phi z}\, c_{\phi y} & c_{\phi z}\, c_{\phi x} + s_{\phi z}\, s_{\phi y}\, s_{\phi x} & -c_{\phi z}\, s_{\phi x} + s_{\phi z}\, s_{\phi y}\, c_{\phi x} \\ -s_{\phi y} & c_{\phi y}\, s_{\phi x} & c_{\phi y}\, c_{\phi x} \end{bmatrix} \tag{2}$$

where: $c_{\phi i} = \cos(\phi_i)$ and $s_{\phi i} = \sin(\phi_i)$, with $i = (x, y, z)$

Table 1 systematizes the parameter sets of the SPRM 3-RRR-type listed previously.

So we have in total 26 parameters for the SPRM 3-RRR-type. In order to maintain the symmetry of the design of the SPRM 3-RRR-type, we consider that $\beta_{1a} = \beta_{1b} = \beta_{1c}$ and $\beta_{2a} = \beta_{2b} = \beta_{2c}$. So we can cut back to 22 parameters.

3. Vertex spaces determination and representation

In order to determine and represent the vertex spaces associated with each SSL, the forward kinematic model of the limb is required to generate the point clouds corresponding to the operational space orientations reached by the MPF as EE of the SSL. These point clouds are obtained as limb forward kinematics mapping of a discretization of the limb joint space. An appropriate representation of the orientations in the operational space is adopted, allowing a consistent interpretation of the orientation capacities. Thereafter, graphical manipulations of the obtained geometric entities in a CAD environment can be efficiently used for workspace and assembly mode determination of the SPRMs.

3.1. Geometric modeling of a spherical serial limb

In this section, we establish the geometric model of each SSL having the MPF as end-effector. The geometric model describing the transformation from the frame of reference O-$X_0Y_0Z_0$, attached to the FB, to the frame E-$X_EY_EZ_E$ attached to the MPF can be formulated using a matrix form. This model set up a relation between join parameters and the operational parameters of the moving platform. The successive transformations (rotations) involved in the forward kinematic model of the serial spherical limb (a), are listed below, see Fig. 2(b):

Fist rotation: beginning with the coordinate system O-$X_0Y_0Z_0$, we make a rotation about the Y_0-axis by the angle ξ so that X_0 is transformed to X_{1a}: the axis of the first revolute joint, see Fig. 1(b). This rotation is expressed by matrix R_{Y0a} in Eq. (3).

Second rotation: it is a rotation about the X_{1a}-axis, see Fig. 1(b), by the angle θ_{1a}, so that the *Z-axis* of the obtained coordinate system (CS) is perpendicular to the plane containing the proximal link of the limb. This rotation is expressed by the matrix R_{X1a} in Eq. (3).

Third rotation: a rotation by an angle β_{1a} about the *Z-axis* of the CS obtained after the 2nd rotation. The angle β_{1a} represents the length of the proximal link. This rotation is expressed by the matrix $R_{Z'1a}$ in Eq. (3).

Fourth rotation: a rotation of an angle θ_{2a} about the *X-axis* of the CS obtained after the 3rd rotation which stands for the axis of the second revolute joint of the limb is realized. This transformation is expressed by the rotation matrix R_{X2a} in Eq. (3).

Fifth rotation: a rotation by an angle β_{2a} about the *Z-axis* of the CS obtained after the 4th rotation. The angle β_{2a} represents the length of the distal link. This rotation is expressed by the matrix R_{Z3a} in Eq. (3).

Sixth rotation: a rotation about the *X-axis* of the CS obtained after the 5th rotation standing for the third revolute joint of the limb is performed by an angle θ_{3a}. This rotation is expressed by the matrix R_{X3a} in Eq. (3).

Seventh rotation: finally, to achieve the configuration of the MPF coordinate system, we perform two successive rotations as follows:

- 7th rotation (a): a rotation by an angle α about the *Z-axis* of the CS obtained after the 6th rotation,
- 7th rotation (b): a rotation by an angle γ_a about the *X-axis* of the CS obtained after the 7th rotation (a).

Remark. the final transformations (7th rotation) are expressed by an inverse (transposed) rotation matrix $\mathbf{R}^{T}_{Ek}$ in Eq. (3).

By using the above successive rotations, we can write the global transformation allowing traveling from frame of reference O-$X_0Y_0Z_0$ to the frame E-$X_EY_EZ_E$ attached to the MPF in terms of the product of the rotation matrices:

$$\begin{aligned}&\mathbf{T}_{OE}^{k} = \mathbf{R}_{Z0}(\upsilon_k)\,\mathbf{R}_{Y0a}(\xi)\,\mathbf{R}_{X1a}(\theta_{1a})\,\mathbf{R}_{Z'1a}(\beta_{1a})\,\mathbf{R}_{X2a}(\theta_{2a})\,\mathbf{R}_{Z3a}(\beta_{2a})\,\mathbf{R}_{X3a}(\theta_{3a})\,\mathbf{R}_{Ek}^{T}\\&\mathbf{T}_{OE}^{k} = \mathbf{R}_{0E} = \mathbf{R}_{Z0}(\phi_Z)\,\mathbf{R}_{Y1}(\phi_y)\,\mathbf{R}_{X2}(\phi_x)\\&\text{with}: k = a, b, c \text{ and } \upsilon_a = 0,\ \ \upsilon_b = 2\pi/3,\ \ \upsilon_c = 4\pi/3\end{aligned} \tag{3}$$

This formulation is applied to the three SSLs (a, b and c). Where, $\mathbf{R}^{\mathrm{T}}{}_{Ek}$ represents the transformation matrix enabling travel from the MPF coordinate system E-$X_EY_EZ_E$ to the three platform local frames attached to the vertices A, B, C, see Fig. 3. For $k = a, b, c$, we obtain the following matrices:

$$\begin{aligned}&\mathbf{R}_{Ea} = \mathbf{R}_x(\gamma_a)\,\mathbf{R}_z(-\alpha)\\&\mathbf{R}_{Eb} = \mathbf{R}_x(-\gamma_b)\,\mathbf{R}_z(\alpha)\\&\mathbf{R}_{Ec} = \mathbf{R}_y(-\alpha)\\&\text{where}: \gamma_a = \pi/6,\ \gamma_b = \pi/6,\ \gamma_c = 0\end{aligned} \tag{4}$$

3.2. Appropriate representation of the orientation operational space of SPRM 3-RRR-type

The key idea of our approach stems from the consideration of an appropriate representation of the operational space. In this representation, the operational space parameters are given by the following set of parameters: ϕ_Z, ϕ_y and ρ. With $\phi_Z \in [0,\ 2\pi[$, $\phi_y \in [-\pi/2,\ \pi/2]$ and ρ is a new operational space parameter which can replace the spin angle ϕ_x introduced in **Section 2**. This new parameter represents a radial distance calculated from the geometric center point of the spherical parallel robot O. In other words, the spin rotation angle around the X_E-axis is replaced by the radius of a sphere centered at point O. ρ varies from $\rho_{\min}$ to $\rho_{\min} + h$ for a variation of the spin angle from 0 to 2π. This parameter can be expressed as follows:

$$\rho = \rho_{\min} + h\frac{\phi_x}{2\pi} \text{ with } \phi_x \in [0,\ 2\pi[\tag{5}$$

In a SCS representation, $\rho_{\min}$ stands for the minimal value, while $\rho_{\max}$ corresponds to the maximal value in the radial direction. The thickness $h = (\rho_{\max} - \rho_{\min})$ can be selected arbitrarily. The coordinates $[X_E,\ Y_E,\ Z_E]^T_{O X_0 Y_0 Z_0}$ of each point in this new orientation operational space can be expressed by multiplying ρ with the first column of $\mathbf{R}_{0E}$, so one can obtain the following expressions:

$$\begin{aligned}&X_E = \rho\,\cos(\phi_y)\cos(\phi_z)\\&Y_E = \rho\,\cos(\phi_y)\sin(\phi_z)\\&Z_E = -\rho\,\sin(\phi_y)\end{aligned} \tag{6}$$

$$\phi_x = 2\pi\,(\rho - \rho_{\min})/h \tag{7}$$

Eqs. (6) and (7) are used to calculate the set of three orientation angles of the MPF associated with the Cartesian coordinates of the FKP solutions with respect to the coordinate system of the fixed base O-$X_0Y_0Z_0$.

4. FKP resolution and assembly modes determination

This section of the article is dedicated to present the technique proposed for resolving the FKP of the SPRM 3-RRR-type.

4.1. Interpretation of FKP resolution and assembly modes finding

As we have mentioned earlier in this paper, the FKP of any parallel manipulator can be formulated as follows: determining the position and/or orientation coordinates of the EECP for given values of the motorized joint variables. In other words, for our case, SPRM 3-RRR-type, when the actuated revolute joints are locked at a set of given input variables, hence the region attainable by each serial spherical limb RRR-type having the MFP as EE is a 2D surface embedded in the 3D operational space defined by ϕ_Z, ϕ_y, ϕ_x. The intersection of these surface regions, for the three limbs of SPRM 3-RRR-type, gives a finite set of points corresponding to the solutions of the FKP attributed to the various assembly modes of the manipulator. This approach should simplify considerably the procedure of the resolution of FKP of the parallel robots because it is based on a graphical procedure where there is no need to develop a numerical polynomial.

4.2. Graphical procedure for FKP resolution

After acquiring the point clouds describing the spatial motion of the EECP belonging to each SSL of the SPRM 3-RRR-type, using the approach presented above in **Sections 2** and **3**, we export it to a CAD package. Below, is the general technique adopted to obtain these 3D geometric entities. Three major steps toward obtaining a 3D freeform surface consist of:

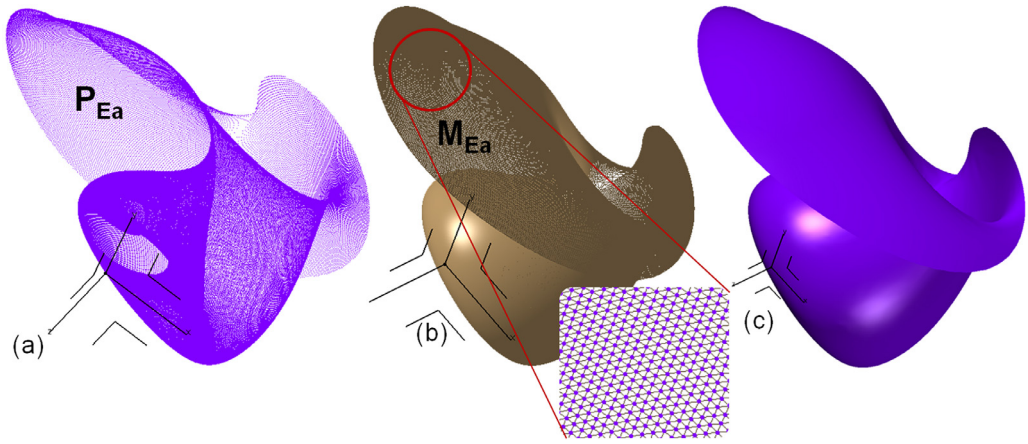

Fig. 4. Imported 3D point cloud of limb *a* describing the spatial motion of the EECP attached to this limb (a), triangular mesh generated on 3D point cloud (b), CAD model of the surface attainable by the EECP associated with SSL RRR-type (c).

(i) *Importing the scattered point clouds data obtained previously in a CAD environment*: 3D point clouds digitized data are exported separately as ASCII files to the CAD package after having obtained it using the numerical phase presented in **Sections 2** and **3** and implemented in MATLAB®.
(ii) *Generation of a polygonal* (*triangular*) *surface mesh*: the 3D polygonal mesh generation process triangles the closest three points in the cloud point until the whole point cloud is networked to form the desired triangular mesh. This process is depicted in Fig. 4(b).
(iii) *Construction of a freeform surface*: the 3D models of the surface envelopes correspond to the spatial motion feasible by the EECP connected to each serial spherical limb.

The above mentioned successive steps are illustrated in Fig. 4 for SSL (*a*).

Remark. In order to guarantee the accuracy of the reconstructed surfaces and the precision of assembly modes determination, each used point cloud contains 250,000 points.

Once we modeled all feasible surfaces of the MPF connected to the different serial spherical limbs RRR-type, we can determine all points associated with the different solutions of FKP (assembly-modes). To realize this goal, we apply two successive intersection operations on the reconstructed surfaces. The graphical operations used to obtain the different points associated with assembly modes are directly performed in CAD environment. These operations can be formulated using the following equations:

$$A_i = S_{Ea} \cap S_{Eb} \cap S_{Ec} \tag{8}$$

In this formula, S_{Ea}, S_{Eb}, S_{Ec} stands for the surface attainable by the EECP when it is considered connected to the first (*a*), second (*b*) and third (*c*) SSL having the MPF as EE respectively, after fixing the first motorized revolute joint in each SSL RRR-type.

The curve resulting from the intersection of two surfaces among three is referred to as the coupler curve feasible by the EECP lies on the MPF of a four bar spherical mechanism RRRR-type. The points associated with the different assembly modes are then obtained after performing the second intersection operation between the curve resulting previously and the third surface. We present the numerical results for the solutions of FKP in the following section of this paper.

4.3. Numerical examples of graphical-based FKP resolution of a general SPRM 3-RRR-type

In this subsection, numerical examples will be presented in order to demonstrate the application of the proposed approach for solving the FKP for SPRM 3-RRR-type.

We consider herein arbitrary designs for the SPRM 3-RRR-type having the geometric design parameters and input joint variables for its actuated revolute joints θ_{1k} ($k = a, b, c$) as shown in Table 2:
where (see Figs. 1, 2 and 3):

β_{1k} stands for the length of the proximal link.
β_{2k} stands for the length of the distal link.
α stands for the semi-angle of the platform cone.
ν_k stands for the rotation angle around Z_0-axis of O-$X_0Y_0Z_0$ to reach the X_{1k}-axis of the first revolute joint in the limb.
ξ stands for the angle between the plane X_0OY_0 and the axis of the first revolute joint of the spherical limb.

Table 2
Geometric parameters and input parameters for SPRMs 3-RRR-type under study.

Geometric design parameters	β_{1k} $(k = a, b, c)$ (deg)	β_{2k} $(k = a, b, c)$ (deg)	α (deg)	υ (deg)	ξ (deg)
Numerical values of the geometric parameters (Robot-1)	45	45	30	120	60
Numerical values of the geometric parameters (Robot-2)	60	60	45	120	22.75
Inputs for actuated joints (Robot-1)	θ_{1a} = -90 (deg)	θ_{1b} = -90 (deg)	θ_{1c} = 30 (deg)		
Inputs for actuated joints (Robot-2)	θ_{1a} = -45 (deg)	θ_{1b} = 135 (deg)	θ_{1c} = -35 (deg)		

Table 3
Six Cartesian coordinates associated with FKP solutions for Robot-1 and the corresponding mobile platform orientations angles, where ($\rho_{min} = 500$, $\rho_{max} = 2500$).

N°	X_E	Y_E	Z_E	Sphere radius ρ	ϕ_Z (deg)	ϕ_y (deg)	ϕ_x (deg)
1	−119.2786119	−479.3251802	−189.984019	529.22012726	256.025952	21.03809	5.259622
2	387.0708477	−201.927861	−350.6160037	559.93775034	332.450008	38.76808	10.78879
3	363.3609312	−464.2342272	−1024.929889	1182.38143689	308.05065	60.09293	122.82866
4	552.2015879	−63.3666373	−1138.869421	1267.26693457	353.45378	63.985301	138.10804
5	−540.8836369	−470.7699204	−1602.396442	1755.52094346	221.03539	65.89176	225.99376
6	−909.9942547	27.5302941	−1575.967815	1820.03352013	178.26714	59.98568	237.60603

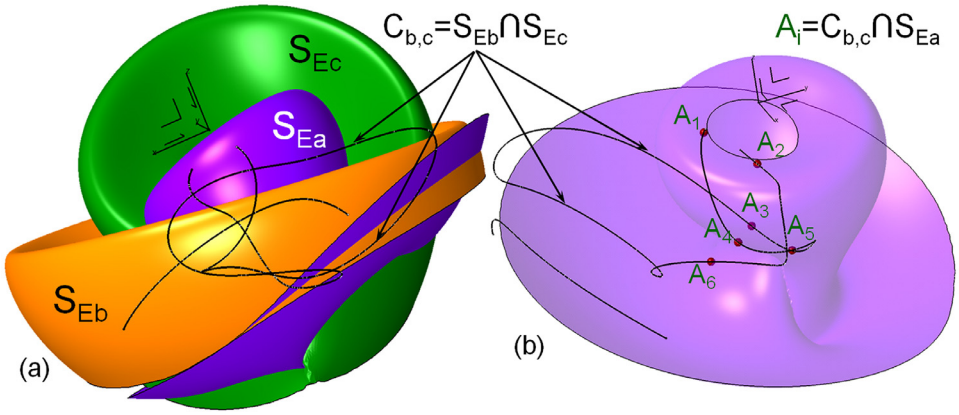

Fig. 5. Resolving the FKP and obtaining the six assembly modes for Robot-1.

4.3.1. Example 1: with six assembly modes

By applying the proposed technique presented in previous sections to Robot-1 (see Table 1); we obtain a set of 6 Cartesian coordinates associated with the assembly-modes. These coordinates are indicated in Table 3. For this robot, the obtained graphical results of the surfaces attainable by the three spherical limbs having the MPF as end-effector are displayed in Fig. 5. Herein, we present also the numerical values of the Cartesian coordinates of its FKP solutions, also the orientation angles of its moving platform corresponding to the obtained FKP solutions. In addition, we display the six assembly modes of this SPRM associated with the acquired FKP solutions depicted in Table 3. Fig. 6 illustrates the MPF of this robot associated with its six FKP solutions. Fig. 6 shows the CAD models of the homothetic SPRM 3-RRR-type corresponding to the obtained FKP solutions.

In order to verify the accuracy of the acquired solutions of the FKP by the use of our approach, we perform a complementary numerical inspection: we measured the angles confined between the unit vectors passing through the axes of revolute joints attached to the MPF and those passing through the axes of the intermediate revolute joints in the SSLs. The results are depicted in Table 4.

4.3.2. Example 2: with eight assembly modes

In this example, we apply the approach developed in this paper for Robot-2 in Table 2. For this SPRM, Fig. 7 shows the 3D CAD models of the surfaces describing the motion of the EECP attached to each SSL of the robot, and the obtained solutions of its FKP. This robot design, with the choice values for the input parameters of the motorized revolute joints, has eight

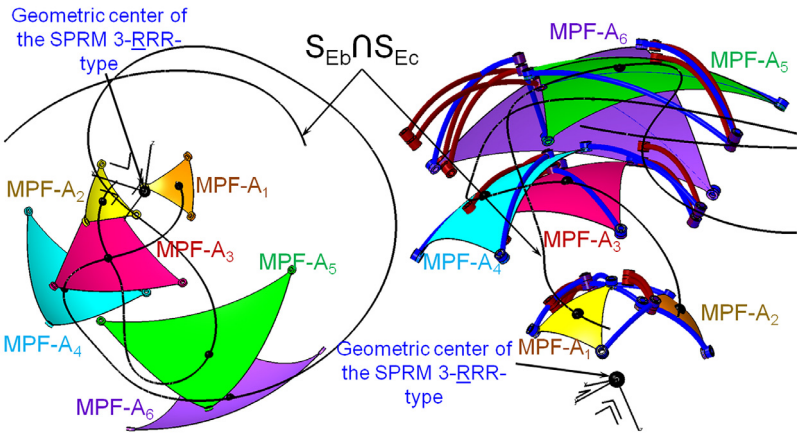

Fig. 6. MPFs of SPRM 3-RRR-type associated with the six solutions of FKP for Robot-1 (left) and the 3D views of the six homothetic assembly modes of Robot-1 (right).

Table 4
Angles between axes of 2nd and 3rd revolute joints in the limb for each FKP solution for Robot-1.

N° solution	β_{2a} (deg)	β_{2b} (deg)	β_{2c} (deg)
1	45.000131642453638	44.999088814281883	44.999055126936490
2	45.000305483415929	44.999486263662277	45.000248897149724
3	44.999215336855499	45.000691756895975	44.997932976208219
4	44.999263059988564	45.000477139113897	44.997908604869522
5	45.001163337884037	45.000436737691857	45.000494171561670
6	45.000217472783156	45.001012163188825	44.999588372361323

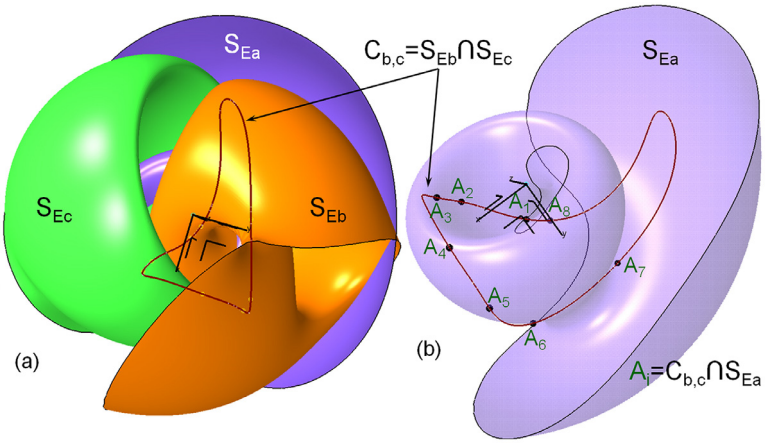

Fig. 7. Resolving the FKP and obtaining the eight assembly modes for Robot-2.

Table 5
Eight Cartesian coordinates associated with FKP solutions for Robot-2, with the corresponding mobile platform orientation angles, where ($\rho_{min} = 500$, $\rho_{max} = 2500$).

N°	X_E	Y_E	Z_E	Sphere radius ρ	ϕ_Z (deg)	ϕ_y (deg)	ϕ_x (deg)
1	308.645083	198.662207	−552.230674	663.08911758	32.76772	56.38901	29.35604
2	138.869645	333.132297	−750.184809	832.48973207	67.37068	64.30753	59.84815
3	686.895839	−289.31596	−154.8769	761.25979469	337.15949	11.73867	47.02676
4	806.006163	−416.365937	111.788817	914.05867937	332.68006	−7.02482	74.53056
5	815.823771	189.74976	730.221133	1111.21388629	13.09344	−41.08198	110.01849
6	926.896282	834.295855	387.053396	1305.75519364	41.99025	−17.24277	145.03593
7	850.557714	1151.114246	−374.655679	1479.48616533	53.53932	14.66894	176.3075
8	−126.685121	1106.023136	−1195.147329	1633.31363676	96.53424	47.03176	203.99645

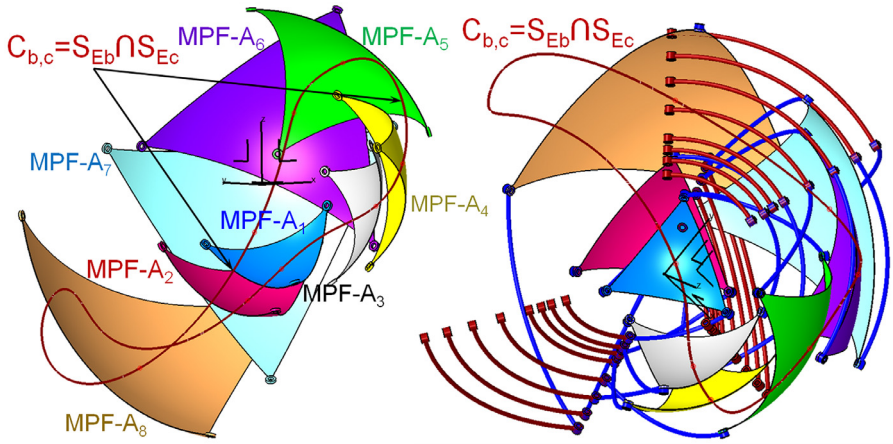

Fig. 8. 3D views of the eight homothetic representations of the assembly modes for Robot-2.

solutions for its FKP (Table 5), as shown in Fig. 7(b). The CAD models of the homothetic SPRM 3-RRR-type corresponding to the FKP solutions are shown in Fig. 8.

We have computed the error on the obtained FKP solutions using the formula presented in [9]:

$$\varepsilon = \frac{1}{n}\left[\sum\left(\cos\left(\beta_{2k}\right) - \cos\left(\delta\right)\right)\right] \quad \text{with } \delta = 45 \text{ deg for Robot} - 1 \text{ and } \delta = 60 \text{ deg for Robot} - 2 \tag{9}$$

where, n stands for the number of assembly modes. The error computed for our approach is $\varepsilon = 9.35 \times 10^{-6}$. This error is comparable to those obtained in [9] $\varepsilon = 4.5 \times 10^{-6}$ by using a semi-graphical method, and in [11] $\varepsilon = 9.1 \times 10^{-6}$ by employing a pure numerical polynomial method as reported in [9].

Remark. for more details, we have added in the appendix the assembly modes obtained previously for Robot-2 using a prototype made by using 3D printing technology (additive manufacturing).

5. Workspace determination and representation of SPRM 3-RRR-type

In this section, we propose a set of approaches, based on the methodology presented previously in this paper, for the determination and characterization of the 3D total orientation workspace (TOW) of the SPRM 3-RRR-type.

5.1. Determination of 3D TOW of SPRM 3-RRR-type

In fact, SPRM 3-RRR-type is one of the parallel manipulators having several solutions to its Inverse Kinematic Problem (IKP) which we refer to as working or functioning modes. For these types of mechanisms, the workspace boundaries are defined by the so-called serial singularities as cited in [14]. So, the central idea in our approach to obtain a 3D total orientation workspace representation of SPRM 3-RRR-type resides in finding the region attainable by the EECP attached to each leg for all the orientations of the moving platform. These regions, embedded in 3D space, are completely confined in the surface envelopes associated with the serial singularities. The SPRM 3-RRR-type 3D TOW is then the common region arising from computing intersection upon the three 3D feasible regions (vertex spaces) of the three serial spherical legs having the moving platform as end-effector. The joint space of each serial chain, isolated from the entire parallel mechanism, can be expressed as follows:

$$W_{JS} = [q_{1,\min},\ q_{1,\max}] \times [q_{2,\min},\ q_{2,\max}] \times \cdots \times [q_{n,\min},\ q_{n,\max}] \tag{10}$$

$q_{i,\min}$, $q_{i,\max}$ stand for the minimum and maximum limits of the joints forming the kinematic chains.

Moreover, the vertex space W_{OSi} of a SSL separated from the rest of the parallel robot can be obtained by solving the FKM for the entire joint space of each limb. FKM stands for the forward kinematic model of the serial kinematic chain for the robotic manipulator. Subsequently, the operational space of the mobile platform of the parallel robot when considering all SSLs connected to form the parallel robotic manipulator can be obtained by the intersection of all vertex spaces attainable by the SSLs having the MPF as EE:

$$W_{OS(Parallel)} = \bigcap_{i=1}^{p} W_{OSi(Serial)} \tag{11}$$

where p: stands for the number of SSLs in the parallel robot. In our case, for SPRM 3-RRR-type we have $p = 3$.

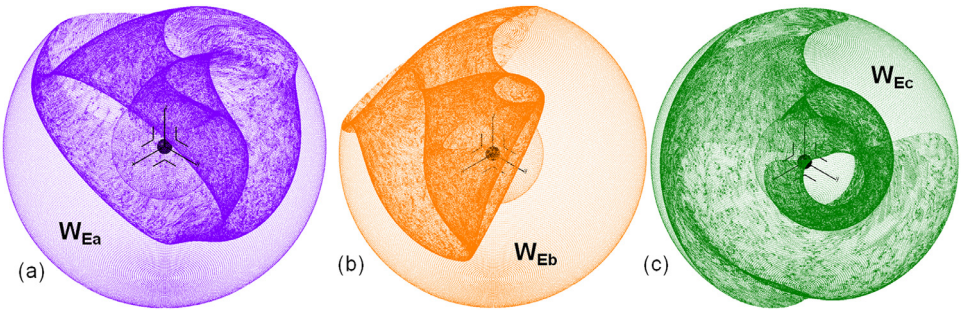

Fig. 9. 3D views of the point clouds for vertex spaces for Robot-2.

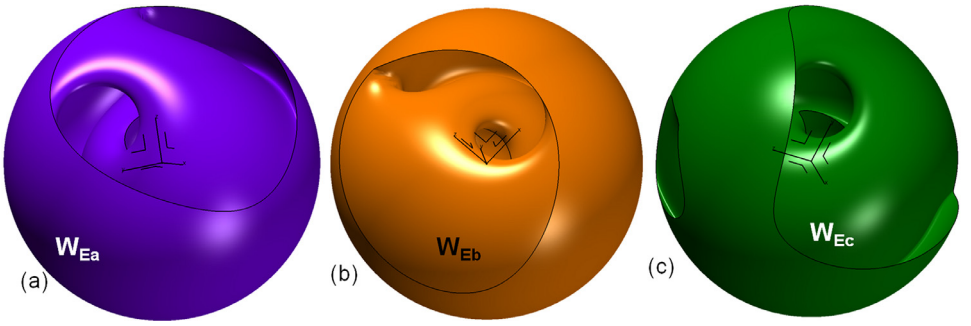

Fig. 10. 3D vertex space achievable by the EECP connected to each serial spherical leg for Robot-2.

5.2. Reconstruction of the 3D TOW of SPRM 3-RRR-type

Numerically, with the aim of acquiring the vertex volumes of SSL having the MPF as EE, we have employed the same procedure presented earlier in **Sections 2** and **3**, by considering the value of the second revolute joint (intermediate one) for each limb RRR-type at two values: $\theta_{2k}=0$ and $\theta_{2k}=\pi$ (where $k=a, b, c$) corresponding to the extended or folded configuration of each SSL of the SPRM 3-RRR-type. The following is the graphical methodology is used to determine the 3D TOW of SPRM 3-RRR-type, which is similar to the one used in the case of FKP resolution:

i Importing 3D scattered point clouds given by the FKM of each SSL having the MPF as EE.
ii Generating the 3D surfaces meshes.
iii Reconstructing the surface envelopes associated with 3D motion feasible by the MPF attached to each leg separated from the rest of the mechanism.
iv Performing a filling operation, in CAD environment, to fulfill the restricted area between the previously obtained internal and external envelopes corresponding to $\beta_{1k} \neq \beta_{2k}$.
v Applying two successive intersection Boolean operations on the 3D reconstructed volumes. This later process allows us obtaining the common solid region associated with the 3D TOW of the SPRM 3-RRR-type. The last step can be expressed as follows:

$$W_{TOW} = W_{Ea} \cap W_{Eb} \cap W_{Ec} \tag{12}$$

Remarks.

1 In this work, we consider that $\beta_{1k}=\beta_{2k}$, for this reason we obtain just one closed envelope surface associated with each 3D vertex space.
2 The internal and external envelope surfaces are obtained for $\beta_{1k} \neq \beta_{2k}$, but the closed envelope surface is obtained for $\beta_{1k}=\beta_{2k}$ as well. These surfaces envelopes correspond to the serial singularities surfaces of each SSL.

5.3. Example of TOW determination

For Robot-2 having the design parameters depicted in Table 2, one can obtain the following results for the 3D TOW (see Figs. 9–11). Fig. 9 shows the 3D envelop point clouds which confine the vertex spaces within it. Fig. 10 depicts the three solid volumes (vertex spaces) reached by the EECP connected to each serial spherical limb RRR-type. The application of the intersection Boolean operations on 3D vertex spaces for obtaining the 3D TOW of Robot-2 is illustrated in Fig. 11.

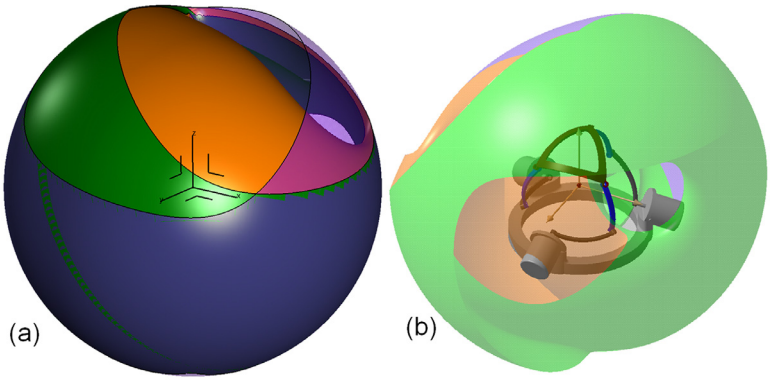

Fig. 11. Application of the first Boolean operation (a), application of 2nd intersection Boolean operation (3D total orientation workspace) for Robot-2 (b).

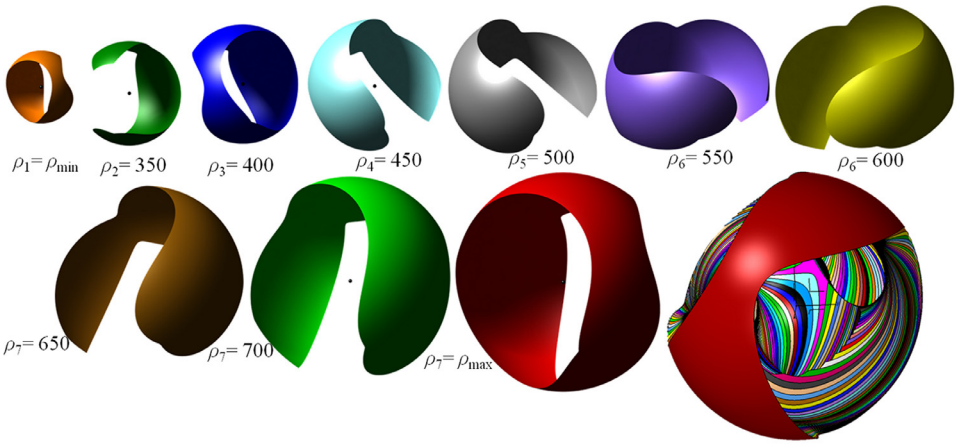

Fig. 12. Constant-spin orientation workspaces of the SPRM 3-RRR-type (Robot-2).

6. Applications to workspace analysis of SPRM 3-RRR-type

6.1. Determination of the constant-spin orientation workspace (CSOW)

After obtaining the 3D total orientation workspace (TOW), (see Fig. 11), one can extract the constant-spin orientation workspace for any fixed desired value of the spin angle ϕ_x of the MPF. The surface representing a constant-spin orientation workspace is obtained by the Boolean intersection between the TOW volume and the sphere corresponding to the spin angle ϕ_x.

The determination of this type of workspace for the SPRM 3-RRR-type will be useful for several applications that require performing specific orientation movements with a constant value of the rotation spin angle.

Fig. 12 illustrates some spherical slices corresponding to different constant-spin orientation workspaces for Robot-2 (Table 1). These workspaces are determined for the following values for the spin angle ϕ_x (deg): 0 corresponds to $\rho_{min} = 240$, 79.2, 115.2, 151.2, 187.2, 223.2, 259.2, 259.2, 295.2, 331.2, and 360 (deg) corresponds to $\rho_{max} = 740$. In addition, a superimposing of all these slices is depicted below on the right of Fig. 12.

In order to compare orientation capacities for different spin angles, the areas of the surfaces corresponding to constant-spin orientation workspaces can be normalized relatively to the spin angle: all these surfaces can be brought back to the same supporting sphere with unit radius. Therefore, the comparison can be performed between normalized areas. Normalized area measurements are represented in Fig. 13 according to the spin angle for Robot-1 and Robot-2 respectively. The obtained graphs have a remarkable periodical feature: the normalized area of the constant-spin orientation workspace evolves periodically with 3 periods over the [0–360°] interval. This may be explained by the fact that the two robots have 3-fold rotational symmetry, as depicted in Fig. 13.

Also, we can conclude according to these graphical illustrations that: for Robot-1, the EECP covers spherical sections with areas between 0.196 and 0.234 over the unit sphere. For Robot-2: the EECP covers spherical sections with areas between

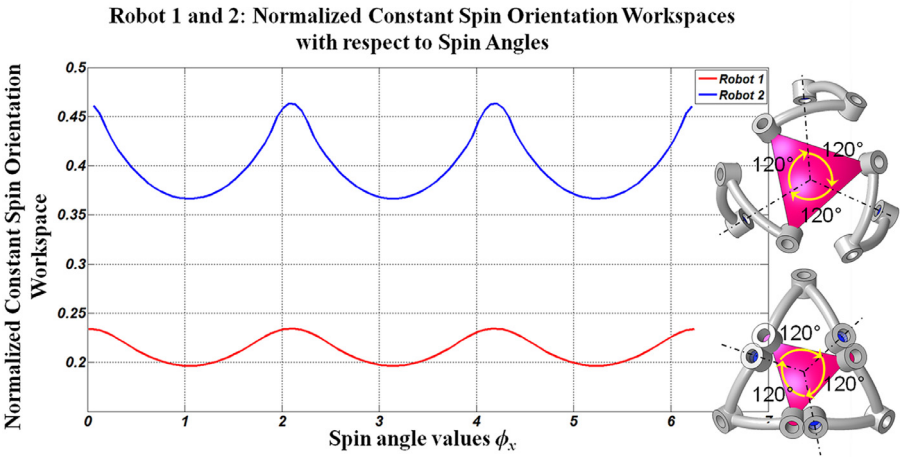

Fig. 13. Evaluation of the areas of constant-spin orientation workspaces with respect to the spin rotation angles ϕ_x, for Robot-1 (red curve) and Robot-2 (bleu curve). (For interpretation of the references to color in this figure legend, the reader is referred to the web version of this article.)

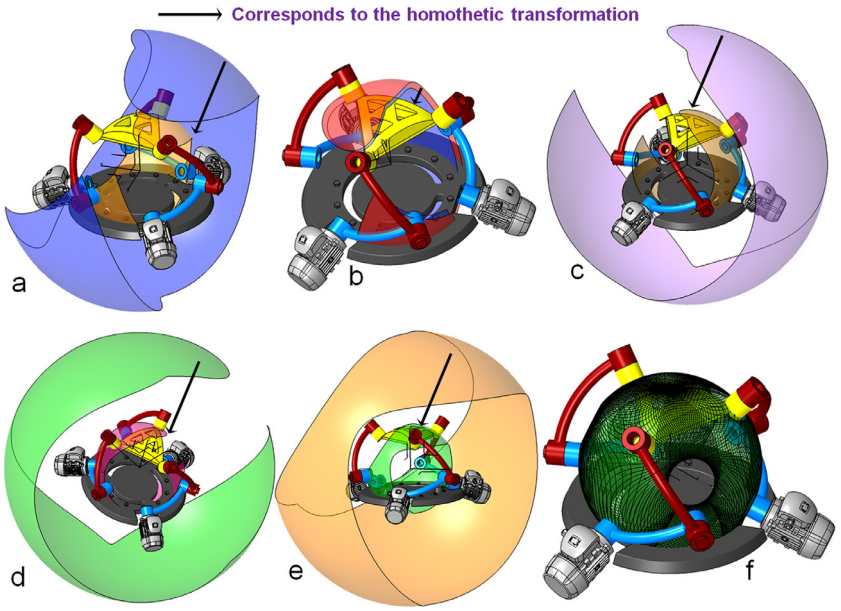

Fig. 14. Applying the homothetic transformation on constant-spin orientation workspaces (a–e), all constant-spin orientation workspaces in the robot scale (f) (for Robot-2).

0.36 and 0.46 over the unit sphere. Consequently, Robot-2 having the geometrical parameters defined in Table 2, can achieve a more important constant-spin orientation workspace than Robot-1.

6.2. Determination of the full-spin orientation workspace (FSOW)

The Full-Spin Orientation Workspace (FSOW) can be defined as the region attainable by the MPF for any spin rotation angle of the MPF of the robot. This type of workspace can be considered as a particular case of the dexterous workspace of a robot. By definition, the dexterous workspace is the set of locations (points) of the EECP for which all orientations are possible [19], or as the volume within which the EECP can be reached with a desired orientation [20]. Thus, according to the previous definitions, the dexterous orientation workspace is considered as a subset of the robot's total orientation workspace. The dexterous orientation workspace is of crucial importance in characterizing the orientation capacity of a SPRM and determining worthwhile applications requiring large spin motions. The technique we propose to extract the dexterous region of the previously obtained 3D TOW is based on the use of the CSOWs as an intermediate step. Herein, we use Robot-2 as an example. This technique can be implemented using the following steps.

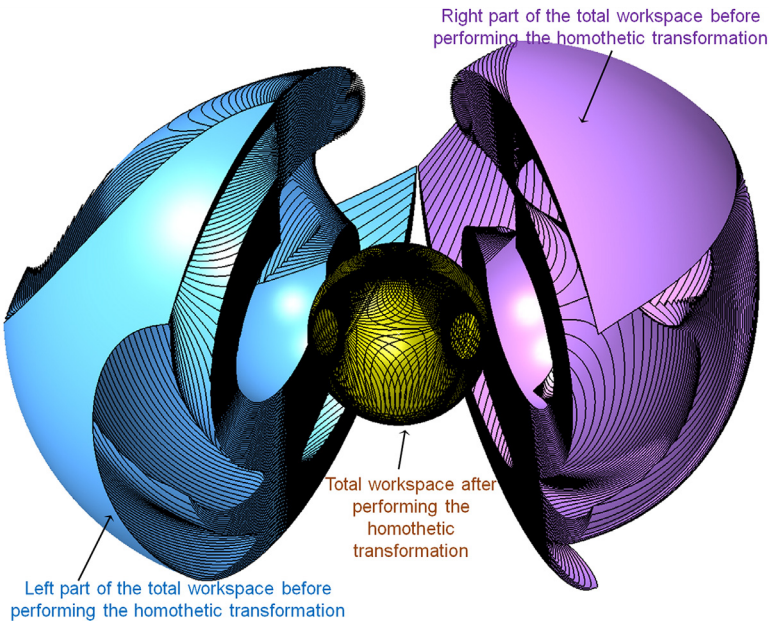

Fig. 15. Anatomic view of workspaces.

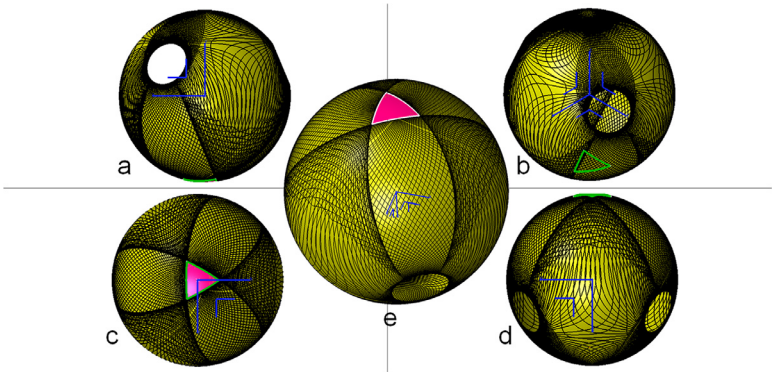

Fig. 16. Common surface corresponding to the FSOW for Robot-2.

- First of all, we determine several spherical slices which correspond to different CSOWs. The interval between two successive spherical sections is denoted by δ ($\delta = 5$ for example). Herein we consider that $\rho_{min} = 240$, $\rho_{max} = 740$. Therefore, $\delta = 5$ corresponds to $\phi_x = 3.6$ deg. Consequently, we have a total of 100 slices that correspond to different spin orientation workspaces (see Fig. 12).
- Thereafter, we apply a homothetic transformation on each spherical slice (constant-spin orientation workspace) to bring it back on to the sphere at the scale of the robot having $\rho = 240$, as illustrated in Fig. 14 for some selected slices. For better comprehension, we have created an exploded view of these surfaces before and after applying the homothetic transformation (see Figs. 14 and 15).
- By considering all these surfaces on the same supporting sphere, after performing the homothetic transformations, it becomes easy to identify a common region corresponding to the intersection between the surfaces. This region corresponds quite simply to the full-spin orientation workspace if the number of surfaces tends to infinity, see Fig. 16.
- Then, this surface can be used to determine the three-dimensional FSOW. To this end, we sweep this surface radially to obtain the volume corresponding to the 3D full spin dexterous workspace, as depicted in Fig. 17.

In Fig. 18, we present the FSOW using the procedure illustrated above for Robot-1 having the design parameters indicated in Table 2.

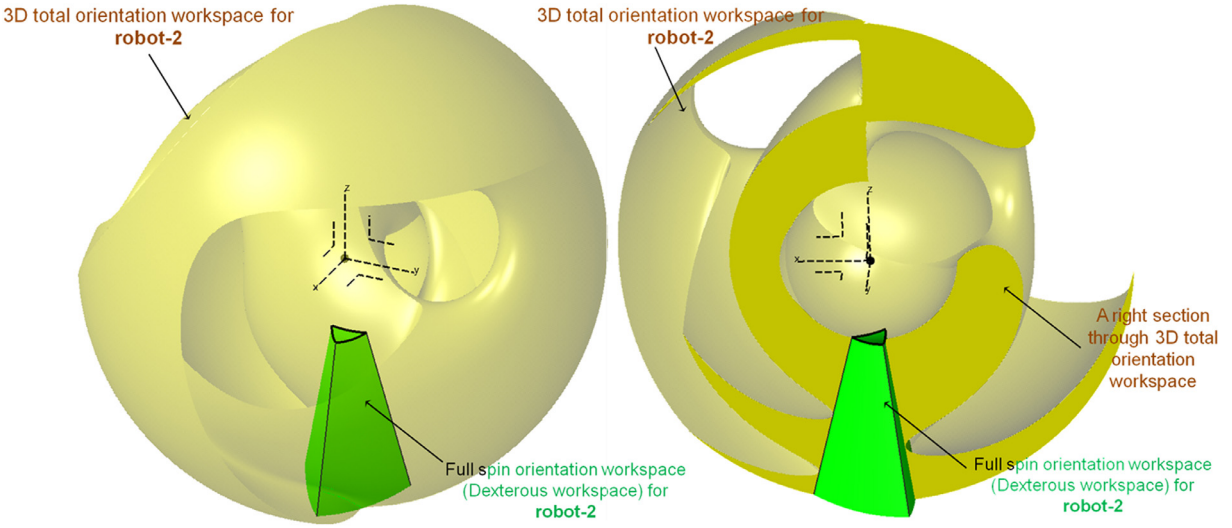

Fig. 17. Obtaining the 3D dexterous workspace for Robot-2.

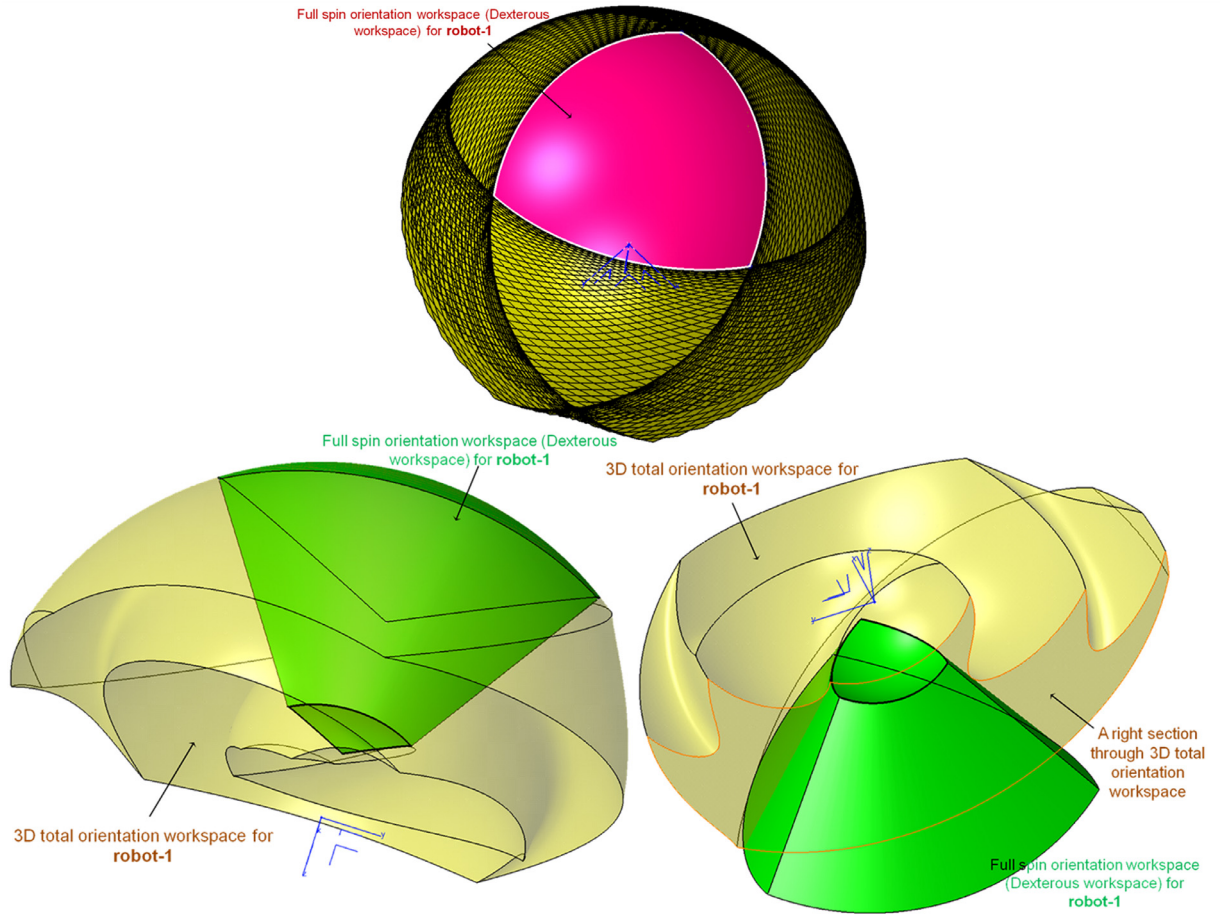

Fig. 18. Obtaining the 3D dexterous workspace for Robot-1.

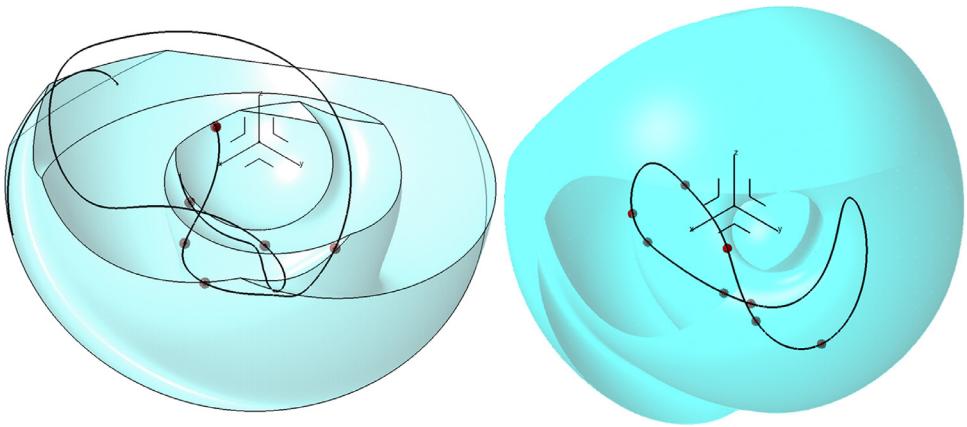

Fig. 19. Superimposing the solutions of FKP (Assembly modes) on the 3D TOW for Robot-1 (left) and Robot-2 (right).

7. Advantages of the proposed methodologies for both workspace representation and FKP resolution of SPRM 3-RRR-type

In this section, we aim to highlight some points showing the relevance and the advantages of the techniques developed for FKP solving and 3D workspace representation and characterization for SPRMs 3-RRR-type:

The classical univariate polynomial approach for FKP has significant drawbacks for some time. We can cite for example, the algorithmic singularities and ill-conditioning [21]. The singularities arise when the tan-half-angles are introduced for obtaining the characteristic univariate polynomial for FKP resolution for example. In other terms, when the tan-half identities are employed, an algorithmic singularity is obviously introduced when the angle value is equal to π. In this context, the transformations based on the use of such identities are frequently performed to obtain one single univariate nth degree polynomial equation. In the case of general SPRMs, one can obtain an 8th order univariate polynomial. The roots of this polynomial represent the solutions sought of the FKP. In addition, the coefficients A_i ($i = 0$ to 8) of the 8th degree characteristic equation, see Eq. (13), are functions of the kinematic design parameters of the manipulator and of the actuator angles (input angles). The obtaining of these coefficients is cumbersome [11]; also, the detailed expressions for these coefficients occupy several pages [11].

$$A_8T^8 + A_7T^7 + A_6T^6 + A_5T^5 + A_4T^4 + A_3T^3 + A_2T^2 + A_1T^1 + A_0 = 0 \tag{13}$$

So, in order to overcome the above mentioned drawbacks of the polynomial approaches, we propose in this work an alternative mean for finding all real solutions (roots) of FKP of SPRM 3-RRR-type. Our proposed approach is founded on a geometrical procedure; it facilitates the resolution of the FKP problem of SPRMs. It uses only the forward kinematic models of the robot limbs to generate the associated vertex spaces while the rest of the procedures consist in graphical resolutions and manipulations applied to these geometric entities. In a preliminary design stage, such an approach is relevant and allows visualizing and analyzing efficiently the main properties of the orientation workspace of SPRMs without going through complex algebraic treatments.

By fixing the joint-space variables, we can determine the domains reached by each SSL having the MPF as end-effector in the operational-space as a 2D surface embedded in a 3D vertex space. The intersection points between surfaces are quite simply the solutions of the FKP of the robot. These points are associated with the different assembly modes of the robotic architecture.

Also, the technique developed herein for FKP resolution enables us to determine all real solutions of FKP and simultaneously visualize them within the 3D TOW of the SPRM robot, see Fig. 19.

In addition, using the proposed methodologies, we have obtained using the 3D TOW, a particular type of the dexterous workspace; this workspace can be named as the Full-Spin Orientation Workspace. Also, the approach allows us to visualize the 3D FSOW through the 3D TOW.

We have determined the 3D TOW as the volume obtained after having performing two successive intersection Boolean Operations on the 3D vertex spaces attainable by each SSL having the MPF as EE.

To the best knowledge of the authors of this paper, this is the first time that the workspace determination and FKP resolution are treated in a unified graphical approach.

8. Conclusion

The TOW and the FKP resolution for spherical parallel robots have been revisited in this paper. The main contribution of this paper is to propose an appropriate parameterizing and representation of the orientation space as well as an approach for FKP resolution and 3D workspace representation. The techniques adopted in this paper have two major stages. The first is numerical, and the second is graphical and has been implemented in a CAD environment. The principle of the reported approach is to deduce, from the constraints imposed on each leg, considered separately from the rest of the mechanism,

the geometric entities which describe all the possible locations of EECP that satisfy the leg constraints. Then, the SPRM workspace is constituted by the intersection of all the entities of the serial spherical kinematic chains associated with the legs. The proposed technique enables also the determination of all the real solutions of the FKP for a given design of SPRM parameters and for given actuated joint variables. The computed error on the obtained solutions of the FKP resolution is comparable with the algebraic methods presented in the literatures. In this context, we have to underline that is not our intention to suggest a method being more precise than the other approaches existing in the literature. But, our aim consists in suggesting new graphical approaches for both workspace determination and FKP resolution of spherical parallel robotic manipulator that can be generalized to other robotic architecture.

Moreover, the superposition of the 3D TOW and the real solutions obtained of the FKP resolution in the same graphical interface enable designers to implement trajectory switching between different assembly mode planning. In addition, using the proposed approach, the constant-spin and full-spin orientation workspaces have been determined and identified. Several case studies have been presented to demonstrate the application of our suggested method. In the future works, we seek to take into account the singularity analysis for this type of SPRM in order to generate singularity-free trajectories having the property of switching between different assembly modes.

Acknowledgments

The work presented in this paper is supported financially by the Excellence Laboratory “LabEX” IMobS3of Clermont-Ferrand, and the Research National Agency in France.

Appendix

The figures below demonstrate the eight assembly modes obtained previously for Robot-2 using a prototype made by using 3D printing technology.

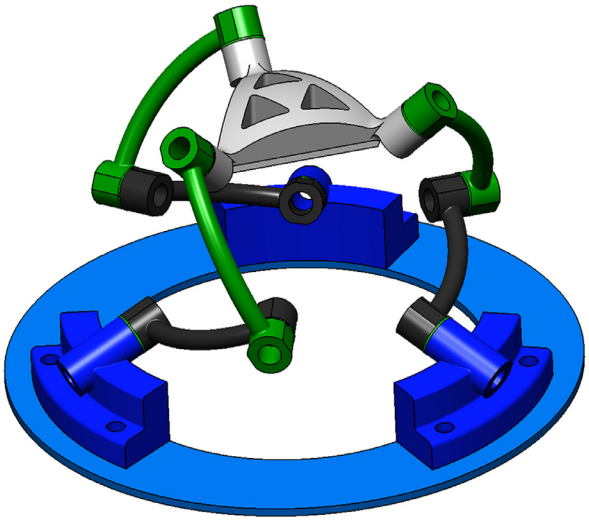

Fig. A.1. CAD model of SPRM 3-RRR-type (Robot-2).

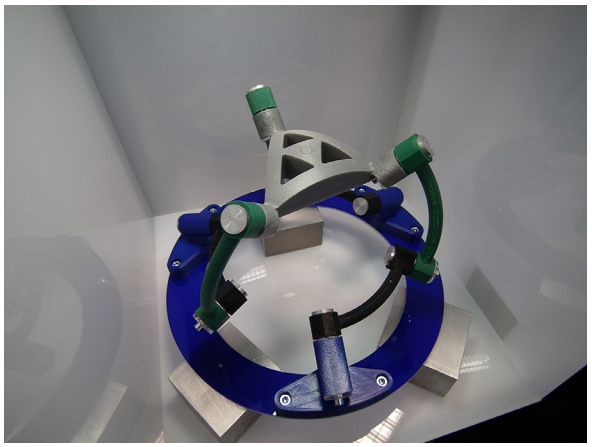

Fig. A.2. 1st view of the prototype of Robot-2.

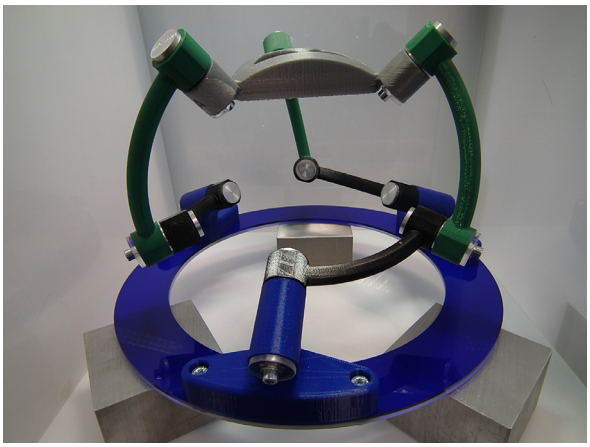

Fig. A.3. 2nd view of the prototype of Robot-2.

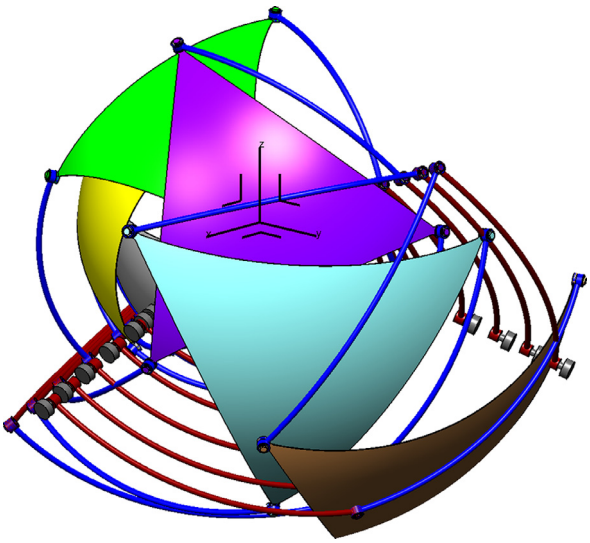

Fig. A.4. 1st view of the 8 assembly modes of Robot-2.

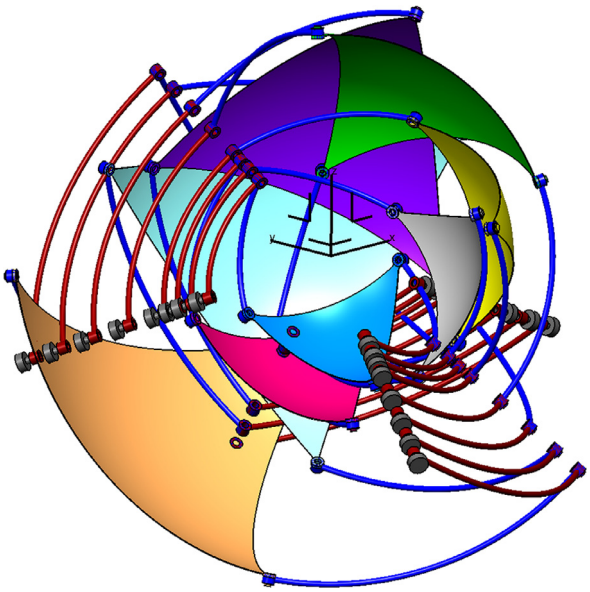

Fig. A.5. 2nd view of the 8 assembly modes of Robot-2.

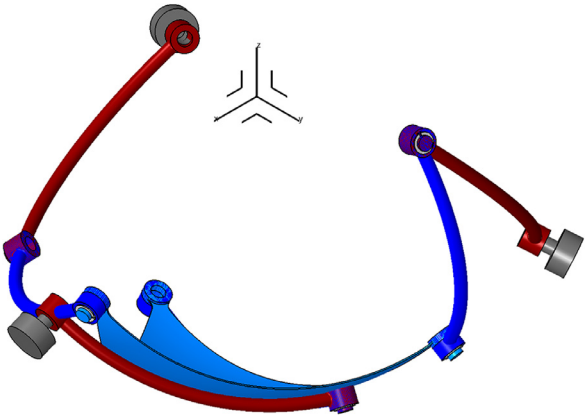

Fig. A.6. CAD model of the 1st assembly mode.

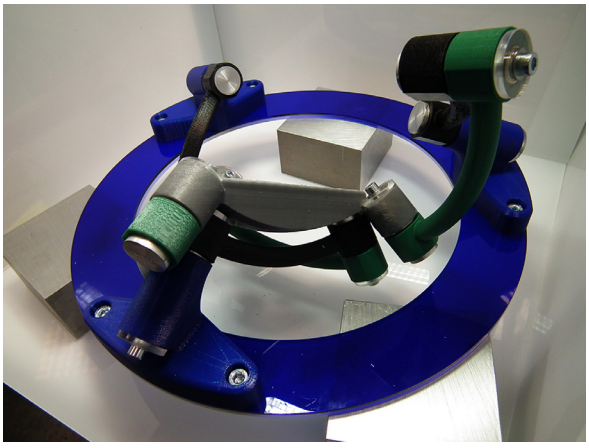

Fig. A.7. 1st view of the 1st assembly mode.

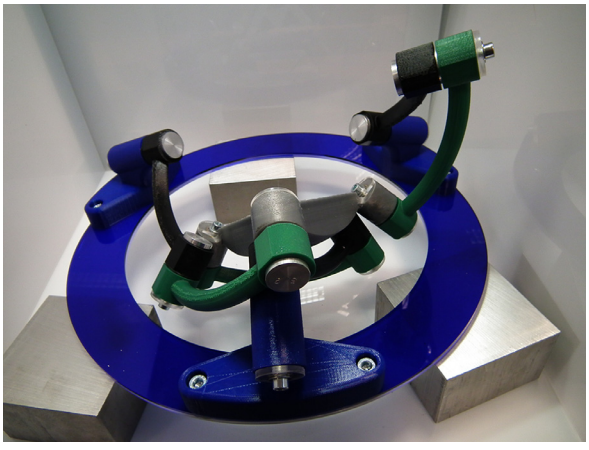

Fig. A.8. 2nd view of the 1st assembly mode.

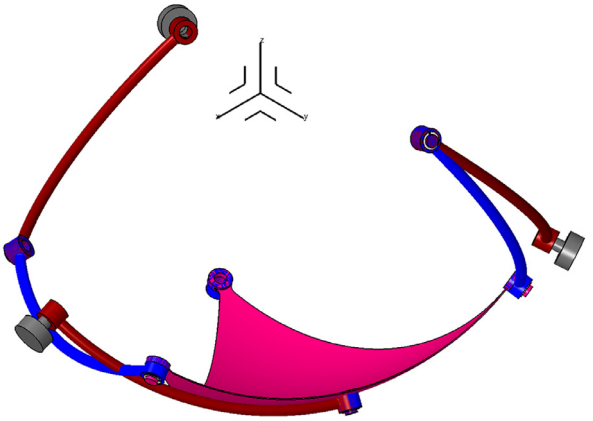

Fig. A.9. CAD model of the 2nd assembly mode.

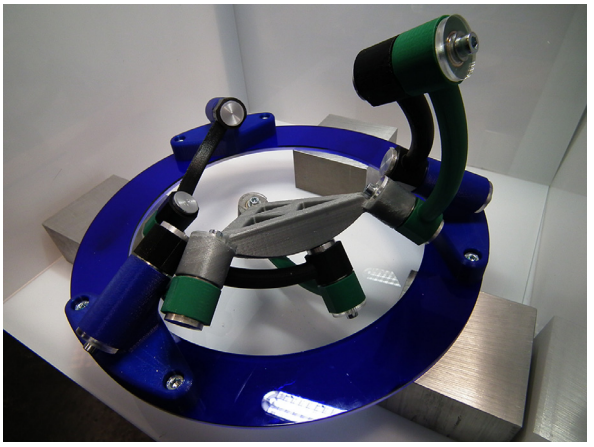

Fig. A.10. 1st view of the 2nd assembly mode.

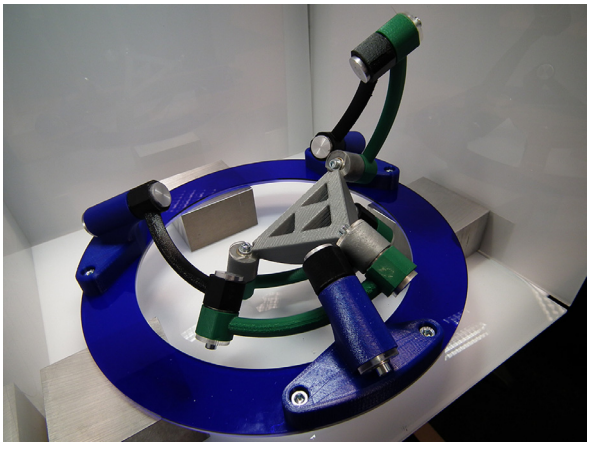

Fig. A.11. 2nd view of the 2nd assembly mode.

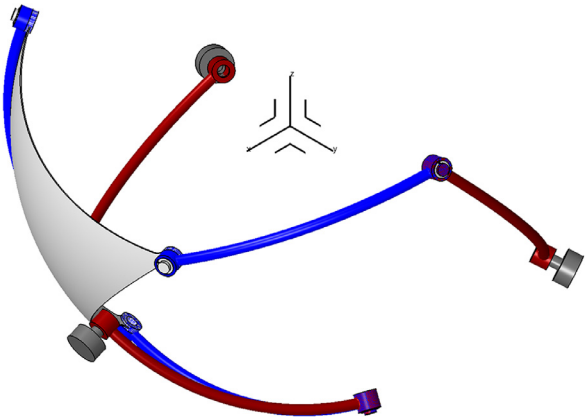

Fig. A.12. CAD model of the 3rd assembly mode.

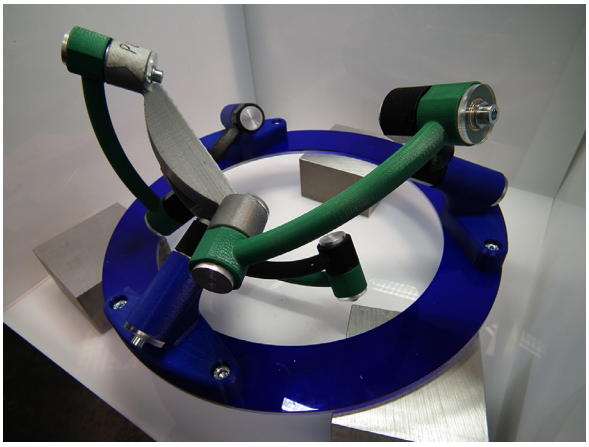

Fig. A.13. 1st view of the 3rd assembly mode.

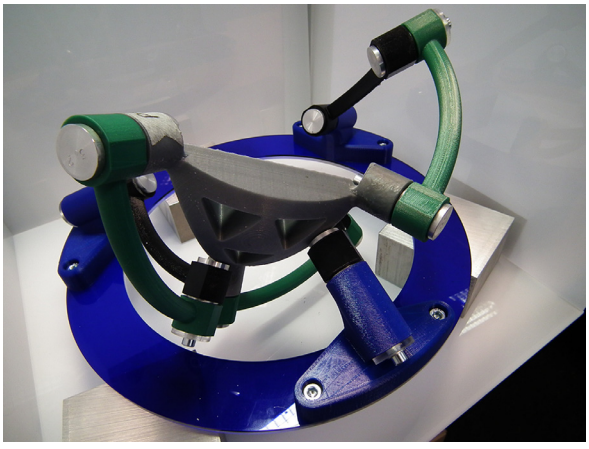

Fig. A.14. 2nd view of the 3rd assembly mode.

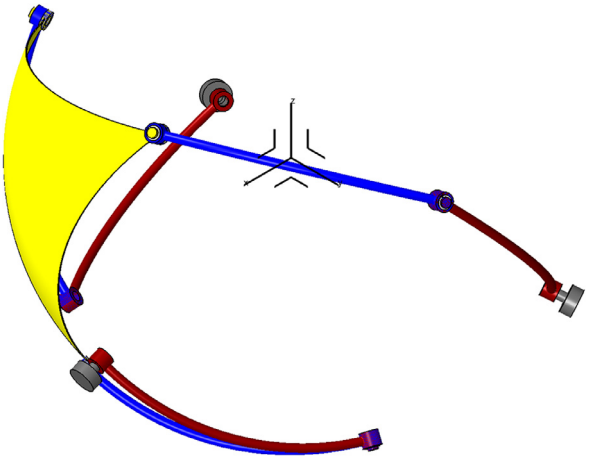

Fig. A.15. CAD model of the 4th assembly mode.

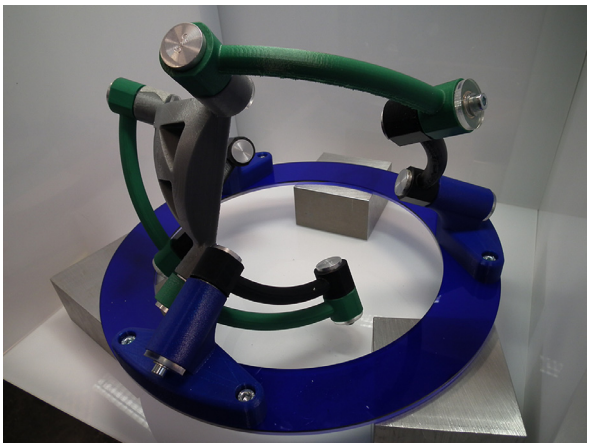

Fig. A.16. 1st view of the 4th assembly mode.

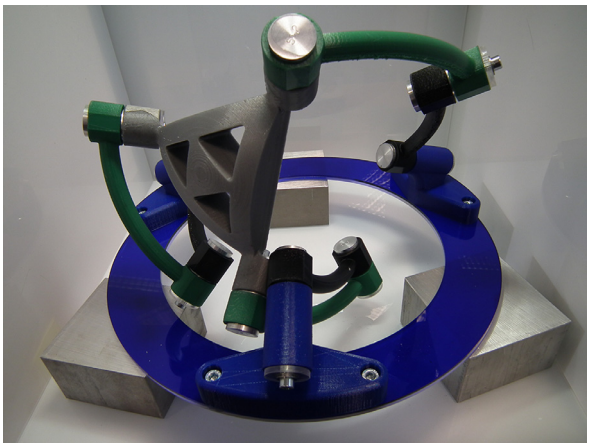

Fig. A.17. 2nd view of the 4th assembly mode.

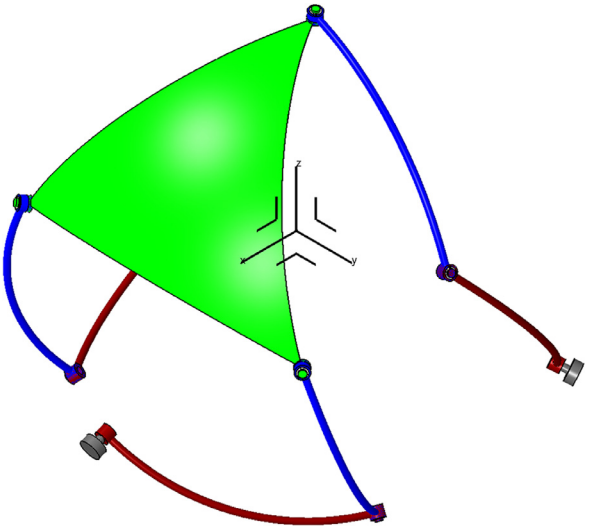

Fig. A.18. CAD model of the 5th assembly mode.

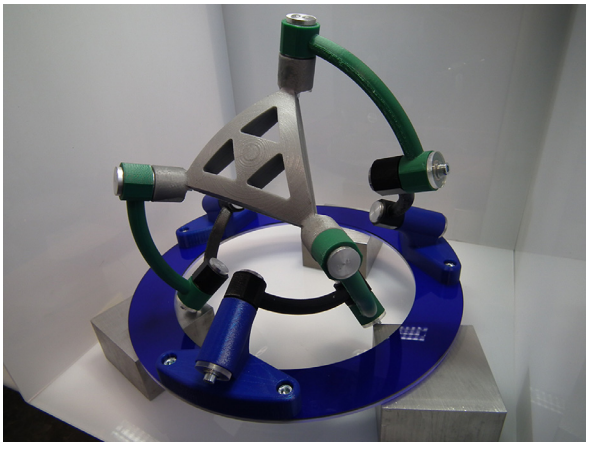

Fig. A.19. 1st view of the 5th assembly mode.

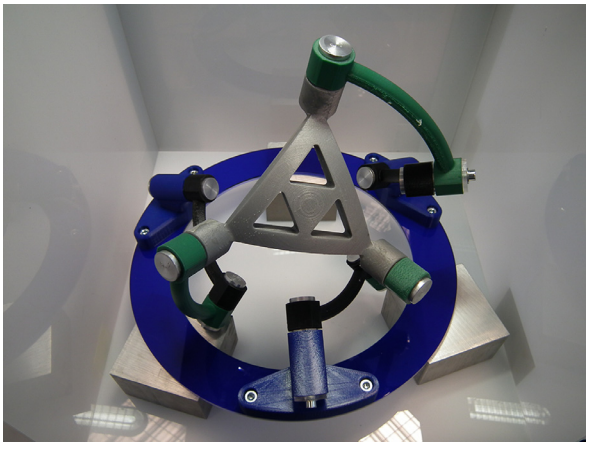

Fig. A.20. 2nd view of the 5th assembly mode.

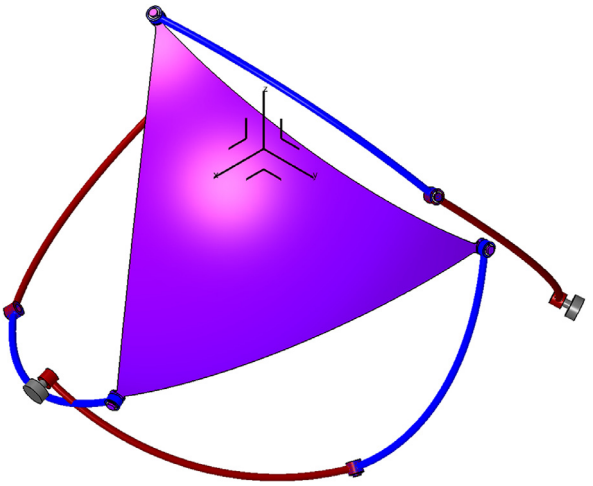

Fig. A.21. CAD model of the 6th assembly mode.

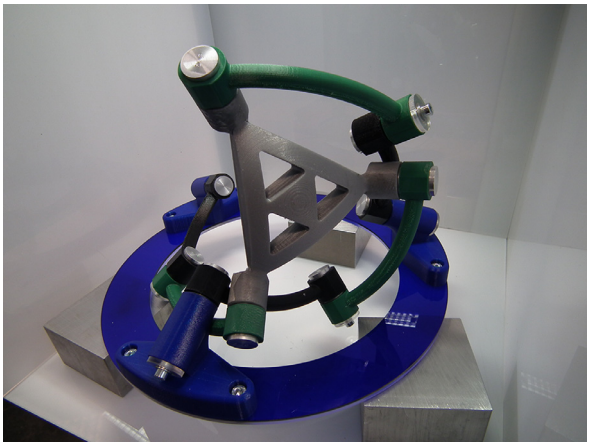

Fig. A.22. 1st view of the 6th assembly mode.

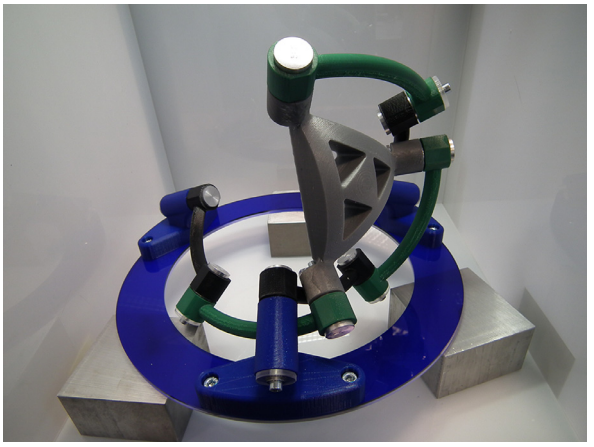

Fig. A.23. 2nd view of the 6th assembly mode.

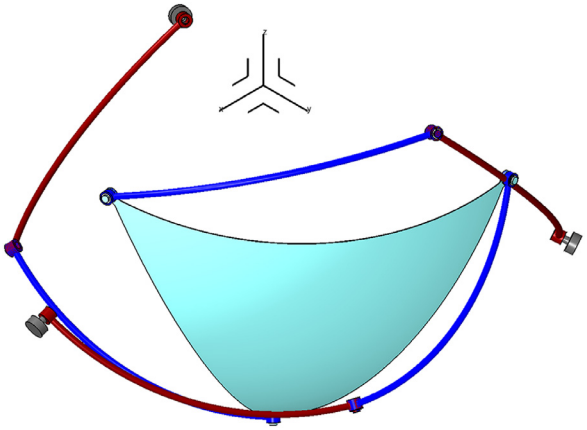

Fig. A.24. CAD model of the 7th assembly mode.

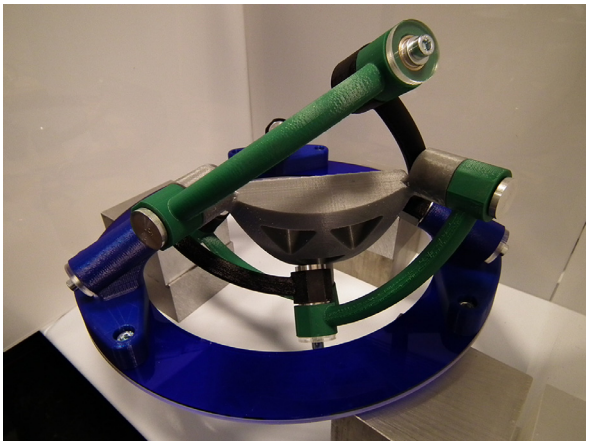

Fig. A.25. 1st view of the 7th assembly mode.

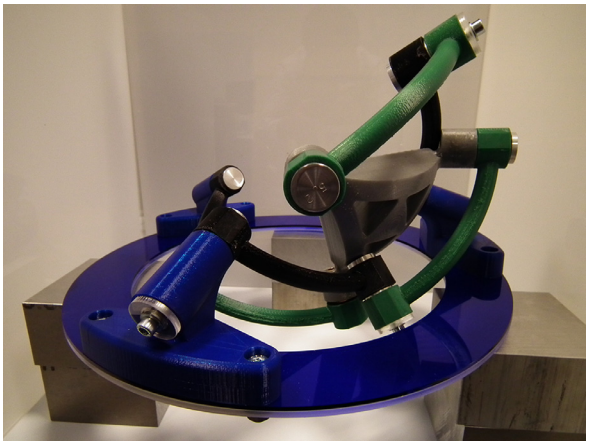

Fig. A.26. 2nd view of the 7th assembly mode.

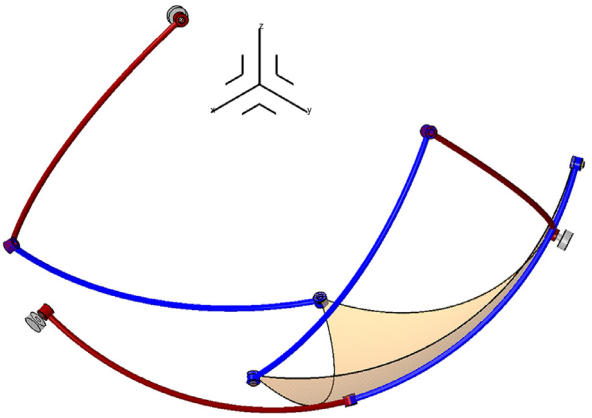

Fig. A.27. CAD model of the 8th assembly mode.

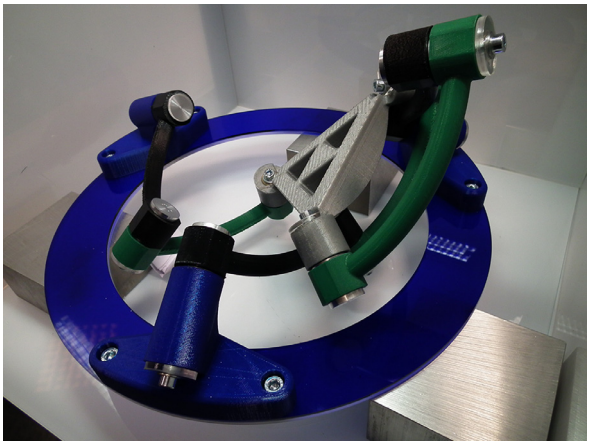

Fig. A.28. 1st view of the 8th assembly mode.

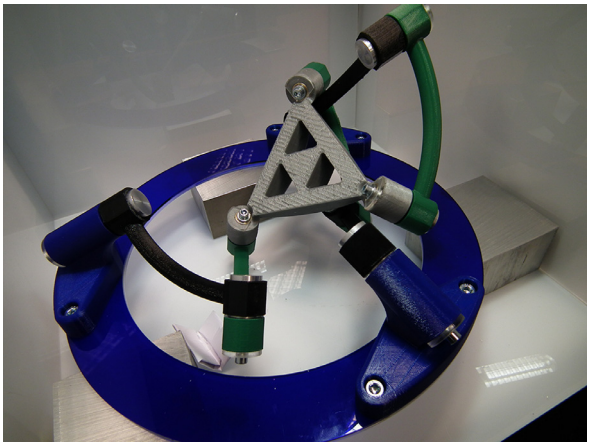

Fig. A.29. 2nd view of the 8th assembly mode.

References

[1] R.M. Murray, Z. Li, S.S. Satry, A Mathematical Introduction to Robotic Manipulation, CRC Press, 1994 ISBN 9780849379819 - CAT# 7981.
[2] I.A. Bonev, C. Gosselin, Analytical determination of the workspace of symmetrical spherical parallel mechanisms, IEEE Trans. Rob. 22 (5) (2006) 1011–1017 Oct, doi:10.1109/TRO.2006.878983.
[3] F. Bulca, J. Angeles, P.J. Zsombor-Murray, On the workspace determination of spherical serial and platform mechanisms, J. Mech. Mach. Theory 34 (3) (1999) 497–512. https://doi.org/10.1016/S0094-114X(98)00019-6.
[4] P.M. Larochelle, Design of 3-DOF spherical robotic mechanisms, in: Nineth World Congress on the Theory of Machines and Mechanisms, 1995, pp. 1826–1830.
[5] B. Ravani, B. Roth, Motion synthesis using kinematic mappings, ASME J. Mech., Trans. Auto. Des. 105 (1983) 460–467, doi:10.1115/1.3267382.
[6] R. Benea, Contribution à l'étude des robots pleinement parallèles de type 6-R-RR-S, Université de Savoie, 1996.
[7] K.A. Arrouk, B.C. Bouzagarrou, G. Gogu, CAD-based unified graphical methodology for solving the main problems related to geometric and kinematic analysis of planar parallel robotic manipulators, Rob. Comput. Integr. Manuf. 37 (2016) 302–321. http://dx.doi.org/10.1016/j.rcim.2015.03.009.
[8] K.A. Arrouk, B.C. Bouzgarrou, G. Gogu, On the workspace representation and determination of spherical parallel robotic manipulators, in: W. Philippe, F. Paulo (Eds.), New Trends in Mechanism science: Theory and Industrial Applications, Springer, 2016, pp. 131–139. ISBN: 978-3-319-44156-6.
[9] S. Bai, M.R. Hansen, J. Angeles, A robust forward-displacement analysis of spherical parallel robots, Mech. Mach. Theory 44 (12) (2009) 2204–2216. https://doi.org/10.1016/j.mechmachtheory.2009.07.005.
[10] C. Gosselin, J. Sefrioui, M.J. Richard, On the direct kinematics of spherical three-degree-of-freedom parallel manipulators with a coplanar platform, ASME J. Mech. Des. 116 (2) (1994b) 587–593, doi:10.1115/1.2919418.
[11] C. Gosselin, J. Sefrioui, M.J. Richard, On the direct kinematics of spherical three-degree-of-freedom parallel manipulators of general architecture, ASME J. Mech. Des. 116 (2) (1994a) 594–598, doi:10.1115/1.2919419.
[12] F. Bulca, M. Husty, Kinematic mapping of spherical three-legged platforms, in: Proceedings of the Fifteenth Canadian Congress of Applied mechanics CANCAM 95, May 28-June 2, 2, Victoria, B.C., 1995, pp. 874–875.
[13] F. Bulca, The kinematics and workspace analysis of platform mechanisms Ph.D. thesis, Dept. Mech. Engineering, McGill University, Montreal, Canada, 1998.
[14] I.A. Bonev, D. Chablat, Ph Wenger, Working and assembly modes of the Agile Eye, in: Robotics and Automation, ICRA 2006, Proceedings 2006 IEEE International Conference on. IEEE, 2006, pp. 2317–2322, doi:10.1109/ROBOT.2006.1642048.
[15] C. Bombin, L. Ros, F. Thomas, On the computation of the direct kinematics of parallel spherical mechanisms using Bernstein polynomials, in: Robotics and Automation, 2001, Proceedings ICRA, IEEE International Conference on. IEEE, 2001, pp. 3332–3337, doi:10.1109/ROBOT.2001.933132.
[16] X. Kong, C. Gosselin, A formula that produces a unique solution to the forward displacement analysis of a quadratic spherical parallel manipulator: The agile eye, ASME Journal of Mechanisms and Robotics 2 (4) (2010) 4, doi:10.1115/1.4002077.
[17] K.A. Arrouk, B.C. Bouzagarrou, G. Gogu, On the resolution of forward kinematic problem using CAD graphical techniques: application on planar parallel robotic manipulators, in: New Trends in Mechanism and Machine Science, Springer International Publishing Springer, New York Cham Heidelberg London Dordrecht, 2015, pp. 43–52.
[18] K.A. Arrouk, Techniques de conception assistée par ordinateur (CAO) pour la caractérisation de l'espace de travail de robots manipulateurs parallèles, Université Blaise Pascal-Clermont-Ferrand II, 2012.
[19] J.-P. Merlet, Parallel Robots (second ed.), Springer, Heidelberg, 2005 ISBN: 978-1-4020-4133-4.
[20] A. Kumar, K.J. Waldron, The workspaces of a mechanical manipulator, J. Mech. Des. 103 (3) (1981) 665–672, doi:10.1115/1.3254968.
[21] L.-I. Gracia Calandin, J. Angeles, in: Robustness to algorithmic singularities and sensitivity in computational kinematics, 225, 2011, pp. 987–999, doi:10.1243/09544062JMES2464.